UNIVERSITÉ DE SHERBROOKE
Faculté de génie
Département de génie mecanique

Isolation et absorption acoustiques à l'aide de mousses actives

Acoustic Isolation and Absorption with Smart Foams

Mémoire de maîtrise
Spécialité : génie mécanique

Abhishek KUNDU

Jury: Alain Berry (directeur)
Patrice Masson
Noureddine Atalla

Sherbrooke (Québec) Canada April 2010

Your file Votre référence
ISBN: 978-0-494-70752-4
Our file Notre référence
ISBN: 978-0-494-70752-4

RÉSUMÉ

Les mousses actives sont des solutions composites de contrôle du bruit qui combinent les avantages complémentaires du matériau en mousse passif et des actionneurs piézo-électriques répartis spatialement à l'intérieur des mousses. Une étude sur le problème de l'amélioration de l'indice d'affaiblissement des mousses actives en utilisant des stratégies de contrôle actif a été effectuée à la fois numériquement et expérimentalement à l'intérieur d'un guide d'onde sous la condition de propagation en ondes planes. Trois différents modèles de prototypes de mousse active ont été pris en compte dans les simulations par éléments finis et leur efficacité à annuler l'onde transmise en aval de la mousse active a été étudiée. Des études expérimentales afin d'optimiser l'indice d'affaiblissement des mousses actives sous une commande prédictive SISO avec un microphone unidirectionnel comme capteur d'erreur démontrent que l'efficacité du contrôle sur une large gamme de fréquences est bonne. Le problème physique de l'annulation de la propagation des ondes sonores est étudié en détail dans les simulations numériques et elles apportent un éclairage précieux sur l'altération de la réponse vibratoire de l'actionneur piézo-électrique de la mousse active sous contrôle optimal. Les résultats des simulations ont aussi contribué à l'identification de stratégies de contrôle de rechange pour l'atténuation de l'onde sonore transmise à l'aide de la réponse sensorielle de l'actionneur distribué. On peut pour cela remplacer éventuellement l'utilisation de microphones en champ lointain et ainsi améliorer notablement la compacité du système de contrôle actif. La réponse sensorielle d'un piezo-actionneur, en raison de sa déformation mécanique est indépendante de la réponse de sa charge totale, avec la compensation analogique-numérique hybride de la "capacite feedthrough" de l'actionneur, à l'aide d'un algorithme adaptatif. Cette charge mécanique de réponse s'est revélé être une bonne approximation de la vitesse radiale du volume de l'actionneur, et peut être utilisée comme signal d'erreur pour maximiser l'indice d'affaiblissement du système de mousse active. En outre, elle a été utilisée dans l'absorption et les problèmes de contrôle TL, fonctionnant sur une erreur de stratégie virtuelle de détection, et a produit les résultats souhaités sur une large plage de fréquences. Le succès du principe capteur/actionneur dans les problèmes de contrôle actif du bruit peut donner des améliorations importantes en termes de positions et de configurations de capteurs d'erreurs associés aux systèmes de contrôle actif.

Mots-cls : Mousses actives, isolation acoustique, contrôle actif du bruit, fx-LMS

ABSTRACT

Smart foams are composite noise control solutions which combine the complimentary advantages of the passive foam material with the spatially distributed piezoelectric actuator embedded in it. Investigation of the problem of improving the transmission loss of smart foams using active control strategies has been done both numerically and experimentally inside a waveguide under the condition of plane wave propagation. Three different designs of the smart foam prototypes have been considered in the finite element simulations and their effectiveness in canceling the transmitted wave downstream of the smart foam has been studied. Experimental studies to optimize the transmission loss of the smart foams under SISO feedforward control with an unidirectional microphone as the error sensor demonstrates good control efficiency over a broad range of frequencies. The physical problem of cancellation of the propagating sound waves is studied in detail in the numerical simulations and they provide valuable insight on the alteration of the vibration response of the piezo-actuator of the smart foam under optimal control. The simulation results have also helped in the identification of alternate control strategies for the attenuation of the transmitted sound wave using the sensory response of the distributed actuator. This can potentially replace the use of far-field microphones and substantially improve the compactness of the active control system. The sensory response of the piezo-actuator due to its mechanical deformation is isolated from its total charge response with the hybrid analog-digital compensation of the quasi-stable feedthrough capacitance of the actuator using an adaptive algorithm. This mechanical charge response has been proved to be a close approximation of the radial volume velocity of the distributed actuator, and has been used as the error signal to optimize the TL of the smart foam system. Additionally, it has been utilized in the absorption and TL control problems, operating on a virtual error sensing strategy, and has been found to produce the desired results over a broad range of frequencies. The success of this piezo-sensoriactuator principle in active noise control problems can provide serious improvements in terms of the positions and configurations of error sensors associated with active control systems.

Keywords: smart foam, acoustic isolation, active noise control, fx-LMS

ACKNOWLEDGEMENTS

First and foremost, I am heartily thankful to my supervisor, Alain Berry, whose encouragement, guidance and support throughout the entire course of my masters have enabled me to develop an understanding of the subject and to explore my research ideas with plenty of freedom.

I would like to thank Yann Pasco for his valuable suggestions and help with the electronic circuits and other hardwares. Thanks are also due, to the valuable advises of Prof. Philippe Micheau with the sensoriactuator circuits.

Special thanks to Mme Chantal Simard for always being very patient with my hardware requirements, and to Mr Patrick Lévesque for fabricating a wonderful and highly precise impedance tube.

I would also like to appreciate the support of all the students of GAUS who have been a wonderful and very supportive lot. Some of whom deserve special mention are Pierre Leroy, Walid Belgacem, Yann Lemonnier and Phani Kiran - the enriching discussions I had with you have been very inspiring.

And definitely cheers to my very good friends - Rokhiya, Bérénice Rey, Carine Havet, Boris Arnaud, Krishna, François Noël, Kyle, Michael Jensen and Asmaa - you are unforgettable. Special thanks to Céline for her abundant patience and effort with the French translations of the abstracts of this work.

My heartfelt gratitude for the continuous support extended to me by my family and friends, who have played a huge role in my formation. I would like to dedicate this work to Danil Chandra Kundu - you are always there with me, grandpa, in the profound serenity of the memory lane.

Finally, I acknowledge the financial support of Natural Sciences and Engineering Research Council of Canada, Bombardier Aerospace, Pratt & Whitney Canada and Bell Helicopter Textron Canada.

TABLE OF CONTENTS

LIST OF FIGURES

LIST OF TABLES

LIST OF ACRONYMS

A list of acronyms used in the present work.

Acronym	Definition
TL	Transmission Loss
SISO	Single Input Single Output
MIMO	Multiple Input Multiple Output
PVDF	Polyvinylidene Fluoride
SPL	Sound Pressure Level
FIR	Finite Impulse Response
IIR	Infinite Impulse Response
LMS	Least Mean Square
fx-LMS	filtered reference Least Mean Square
Cu-Ni	Copper-Nickel
d.o.f.	degrees of freedom
Op. Amp.	Operation Amplifier
CMR	Common Mode Rejection

CHAPTER 1

INTRODUCTION

1.1 General Remarks

Noise and vibration control, in a wide range of industrial and daily life applications, has become a field of intense engineering and scientific interest over the past few decades. The study has been incentivized by environmental considerations, legal compliance, necessity of improving the lifespan of the associated vibrating structures and also due to enhanced personal comfort consideration and increasing commercial interests.

Sound absorbing materials have been in practice for a long time now and they offer the most practical and economic solution in many situations. Generally, all materials have some sound absorbing properties over particular range of frequencies which maybe described by calculating the sound absorption coefficient of these materials. It is possible to classify the sound absorbing material into three broad categories - (a) Porous Absorbers (e.g. fibrous mineral wool, glass fiber, aerated plaster, spray applied cellulose, etc., these are the most commonly used and are efficient in the mid and high frequency range of incident sound, the thickness of these materials have a strong bearing on their sound absorption coefficient), (b) Panel Absorbers (non-rigid non-porous membranes like thin wood paneling over framing, lightweight impervious ceilings and floors etc. which are capable of exhibiting resonance characteristics in response to the excitation sound field, and are most efficient in the low frequency range) and (c) Resonators (some perforated materials and other materials which have openings as a combination of holes and slots, like Helmholtz resonators, and these typically act to absorb sound in a narrow frequency range; also, the resonant frequency is governed by the geometrical dimension of the resonators).

On the other hand, a wide range of active control strategies can also be developed that enables cancellation of a primary sound source by the use of a secondary source and an error microphone. The underlying physical principle is that of interference. The coefficients of the digital filter, that will typically drive the secondary source based on some reference signal correlated to the disturbing noise, are chosen to ensure that the waveform of the sound radiated from the secondary source is aligned in time in order to be (as far as possible) opposite to the waveform produced at the error microphone by the primary source. However, most of the acoustic waveforms of practical interest are highly

unpredictable (like those inside an automobile due to the airflow past the passenger cabin and the vibrations generated by the contact of the tires with the road) and in addition, there may be multiple primary sources of such unwanted sound. In such cases it becomes more difficult to find reference signals that give a prior indication of the acoustic pressure fluctuations well before their arrival. Also, global control strategies have proved to be less efficient compared to local control ones.

However, the idea of improving the overall absorption coefficient of the passive materials over a broad range of frequencies have motivated researchers to combine active components with the conventional passive methods and thus utilizing the complementary strengths of these individual components in developing efficient control strategies and algorithms that can actually reduce the dimensional penalty one has to incur while using the passive components alone (especially at low frequencies). It is also worth mentioning that although many of the physical principles involved in active sound control have long been established, the development of considerably fast and sophisticated digital processors over the past few decades has stimulated the growth and rapid enhancement of the study of active noise control.

Smart foam is a composite noise control treatment consisting of a layer of partially reticulated passive acoustic foam material with a distributed piezoelectric actuator, such as polyvinylidene fluoride (PVDF) embedded in it. The passive foam offers good sound attenuation in the mid and high frequency ranges, while the active piezo-actuator provides a solution for low frequency noise cancellation with the help of active control. Thus the resultant smart foam combines the inherent mid to high frequency passive noise control capability of an acoustical foam treatment with low frequency noise control capabilities of an active control system, and hence implementing the passive sound proofing system as part of the active system to conserve weight and space.

1.1.1 Literature Review: Smart Foam

Acoustic waves incident on the porous material are dissipated due to structural, viscous and thermal losses due to the relative motion of the solid and fluid phases of the foam matrix. However, the inefficiency of these materials to exhibit satisfactory low frequency absorption coupled with the increasing dimensions at these frequencies have motivated the development of smart foams. Low frequency attenuation may be achieved using an appropriate control input applied to the curved layer of the active piezo-material. This active material, when strained under the application of an external electrical voltage, will induce a volume velocity by means of a pumping action. This pumping action normally

results due to the curvature of the distributed actuator which leads to a strong coupling between the in-plane displacement of the active material with the radial out-of-plane displacement. This leads to an operation similar to that of an ordinary loudspeaker, which generates a secondary sound field under appropriate control input.

Thus the 'Smart foams' or 'Adaptive Foams' present a new approach in controlling unwanted noise field and presents manifold advantages over other passive/active noise control solutions. Fuller *et al* [Guigou and Fuller, 1998; Fuller *et al.*, 1996, 1994] have conducted studies on smart foam and demonstrated their effectiveness in sound control applications and the advantages they present over the other hybrid passive/active systems. The configuration of the smart used in their study [Fuller *et al.*, 1994] consisted of cylindrically curved section of PVDF film embedded in partially reticulated polyurethane acoustic foam with an active input to the PVDF element which was driven by an oscillating electrical input. Their study of radiation control was implemented in two steps - first, with a far-field traverse microphone which fed an error signal into the single channel filtered-x LMS control algorithm along with a reference signal from the disturbance, and secondly with a PVDF sensor mounted on the surface of the adaptive foam whose response is used as the error signal to be minimized. A global sound attenuation of approximately 20 dB was achieved with the far-field microphone as the error sensor, while the PVDF film error sensing strategy exhibited no far-field pressure reduction at all. The reflection control experiment was conducted with plane acoustic waves incident on a smart foam placed at one end of a standing wave tube and with two microphones used for estimating the reflected wave intensity using an analog wave deconvolution circuit. The control was accomplished with a fx-LMS algorithm. The reflection control can be interpreted as a process of actively creating an impedance on the surface of the foam (using the embedded PVDF actuator) which matches the impedance seen by the incident plane wave propagating away from the source. Up to 40 dB of attenuation of the reflected wave was achieved at frequencies above 600 Hz while using the active control strategy. At low frequencies between 150 and 300 Hz, the adaptive foam was less efficient but still produced a 10 dB reduction in the SPL. Further development was brought about in 1996 [Fuller *et al.*, 1996], which was devoted to the development and testing of foam-PVDF smart skin for use in aircraft fuselage in order to reduce interior noise associated with the turbulent boundary layer excitation. An improvement in the radiation efficiency of the smart foam was brought about in the paper using the idea of Tibbets [Tibbetts, 1977] and the improved PVDF actuator configuration is shown in Figure 1.1.

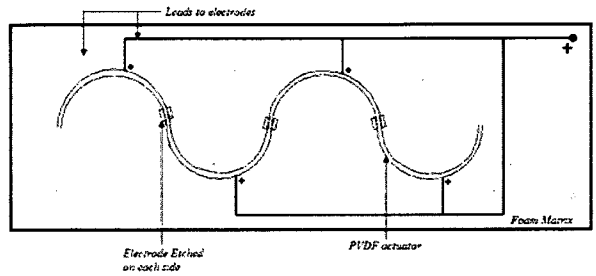

Figure 1.1 PVDF actuator configuration in Parallel [Fuller *et al.*, 1996]

In this improved configuration, the continuous PVDF film was divided into several individual transducers by a chemical etching process. Thus effectively the actuator is composed of several individual transducers connected in parallel which are driven in the opposite directions simultaneously. This results in a higher sound radiation efficiency compared to the previous approaches. This configuration gives global cancellation of harmonic and broadband noise induced by a vibrating piston and it was possible to control SPLs of the order of 60 dB at 300 Hz when applying a maximum allowable voltage (300 Vrms). In order to further improve the radiation efficiency of the system in the low frequency range, to develop more integrated error sensors for compact design and to develop an adaptive feedback controller to avoid the use of a reference signal (necessary in feedforward control), Guigou and Fuller [Guigou and Fuller, 1998] compared the performance of the radiation control smart foam using both the feedforward and the feedback controllers for different disturbance frequency bandwidths. The error signal was provided in both cases by an error microphone located in close proximity of the smart foam. Better results were obtained for the case of adaptive feedback control which is quite expected since the reference signal has to be synthesized. However, for greater frequency bandwidths, the results deteriorate suggesting that an adaptive feedforward controller is more efficient in reducing radiated power over broad frequency bandwidth.

Mathur *et al* [Mathur *et al.*, 2001] have developed a finite element model to meet the design requirements of the smart foams. A 3D model was made for the fluid and the poroelastic domain, while the PVDF film was modeled in 2D. The active control implementation was made in a 2D representation. The experimental validation of their model for the simple cases showed the effectiveness of their model. A number of near field and far field microphones were used for control and measurement, and accelerometers responses mounted on the test panels provided the realistic reference signal. The noise reduction results due to different active control strategies on the test panel and the fuselage section of Boeing 757 demonstrates significant improvement under both acoustic and structural

excitations. The strategy using the far-field minimization was observed to give better results with a reduction of about 7-10 dB in a the frequency band of 200-700 Hz. However, the piezoelectric actuator model was limited to 2D.

A 2D smart foam model was considered in the works of Chin *et al* [Chin *et al.*, 2002] to demonstrate the active control implementation. The arrangement consisted of three smart foam prototypes placed at the termination of an air duct and excited by a line volume velocity (primary source) which represents a noise of 80 dB SPL. Both the global (total acoustic pressure vector set to zero, which in effect aims at minimizing the noise field at every point inside the tube) and local (aims at minimizing the acoustic pressure at certain preselected locations in the tube) noise reduction strategies have been investigated in the paper. The overall reduction ranges from 10 to 40 dB. The local control strategy proved to be more effective than global control, because fewer number of pressure variables had to be minimized for this case. Also, the smart foam placed at the center in the array of the three foams, proved to be more critical in reducing the sound pressure than the other two, and this can be utilized as an advantage in the subsequent control strategy designs.

D'Angelo [D'Angelo, 2004] continued in the line of Fuller and studied the influence of reference sensor and sensor error on the effectiveness of noise control in an airplane cabin. He managed to get attenuations of 16dB on the frequency range 400-800Hz with a configuration of 3 reference sensors and a near field error sensor.

The use of smart foam has also been applied to the control of noise induced by the turbulent boundary layer (TBL) inside the aircraft fuselage in the work of Griffin [Griffin, 2006]. An fx-LMS algorithm was used for the tests. Control was applied at one bay using an arrangement of six smart foam elements configured for a four channel control. Each channel of control had a single accelerometer for providing the reference signal with four microphones, placed 20 inches from the plate, which acted as the error sensors. A reduction of 2 to 5 dB over a control bandwidth of 400-1000 Hz was attained with an average attenuation of 2.5 dB. Passive attenuation achieved by the presence of the foam alone was 3.8 dB over 400-1000 Hz.

Leroy *et al* [Leroy *et al.*, 2007] presented a finite element study of three smart foam prototypes with different designs of the distributed piezoelectric actuators. The prototypes were placed inside impedance tube and the assumption of plane wave propagation was assumed to hold true over the entire frequency range of interest from 100 to 1500 Hz. The melamine foam material used as the passive sound absorbent material offers the advantage of being light weight. The best passive behavior for acoustic absorption was obtained with

the third configuration (having the highest actuator area). Real time adaptive control was implemented using the fx-LMS algorithm, a unidirectional microphone as the error sensor, and the primary source input as the reference signal. The control results show good improvement in absorption coefficient over the frequency range of interest. For harmonic primary perturbation, a perfect absorption coefficient of 1 is obtained at all frequencies for all the three prototypes, while for the adaptive control of white noise (broadband noise), their performance deteriorates. This deterioration has been attributed primarily to the causality constraint of the active noise control system, and also to the possible non-linear effects of the smart foam prototype. The results show that prototype 3 combines the passive/active characteristics of the smart foam quite well and gives an absorption coefficient close to 0.9 from 300 to 1500 Hz.

1.1.2 Main Objectives

The literature review reveals that there have already been some developments in the design of smart foams for absorption and radiation control. However the acoustic transmission control problem with smart foams, still remains a sparsely studied domain, and forms the prime focus of the current work. The main objective of the current work is to enhance the acoustic transmission loss of the passive foam material using the smart foam principle, and to gain an in-depth understanding of the physical mechanism that leads to the above goal.

A complete 3D finite element model of the poroelastic material with the active component integrated to it has been developed at the GAUS laboratory which enables the investigation of the various performance parameters of the smart foam that may prove to be important in terms of their noise attenuation capabilities [Leroy, 2008]. The specific areas of interest of the present study maybe listed as follows.

- **Study of sound transmission loss of the Smart Foam**

The energy indicator selected as the optimization parameter for this problem is transmission loss(TL), which is defined as the ratio of the incident sound power to the transmitted power [Galland *et al.*, 2005]. The present problem is restricted to the study of plane wave propagation in impedance tube, however, the TL energy indicator is equally valid for the general case of diffused field excitation problems. It will be interesting to study the transmission efficiency of these systems under the passive/active operating conditions, where the finite thickness smart foams used for sound absorption purposes can be investigated for the amount of acoustic energy transmitted through them under passive operating con-

ditions. This will basically reflect the transparency of the smart foam systems to the incident sound waves. The modification of the PVDF vibration response, under optimal control, that will result in the cancellation of propagating transmitted sound wave will taken up in detail in the present study. For the absorption control problem, the actuator modifies the surface impedance of the smart foam materials such that the absorption coefficient is enhanced. A comparative study of the absorption problem of with that of transmission control will be considered here which can highlight the complimentary nature of these problems and help to improve the performance of the active noise control system and identify the key design parameters associated with smart foams. It will also be interesting to look into the reflected wave characteristics as the smart foam system is optimized for the transmission loss problem. It does not necessarily hold that maximizing the transmission loss will enhance the acoustic absorption, and hence remains to be investigated.

- **Understanding the physical mechanisms of energy dissipation in smart foam**

The finite element model developed at GAUS is an analysis tool that is capable of providing the information about location and extent of various modes of energy dissipation (like viscous, thermal and structural) in the smart foam prototype. These indicators can allow us to understand better the physical mechanisms of energy dissipation, which will help to recognize the ways to increase the overall absorption of the material. Based on these, it may be possible to put forward important recommendations on the key design parameters. Also comprehensive literatures are available on the models that characterize the behavior of different poroelastic materials, with varying physical properties (using complex impedance and complex wave number expressions). However, the final expressions obtained are often complicated and throws little light on important physical and geometrical parameters that can influence the dissipation phenomenon to the greatest extent. The study of the acoustic energy indicators with the FEM model can provide valuable insight into this aspect and help to identify the key optimization methods.

- **Sensors**

The design and position of sensors is always an important consideration in smart foam configurations owing to the requirement of efficient control algorithm and compactness of the system. It can be seen from the above literature survey that the position of sensors in the acoustic field is critical to the performance of the active control system, it is desirable that the sensors are located close to the smart foam prototypes. However, the acoustic near field may pose significant problems in this implementation. Unidirectional microphones

are generally used for the purpose of sensing the acoustic pressure which serves as the reference signal as well as the error signal in the absorption control experiments inside the impedance tube. It will be interesting to investigate the possibility of deriving the control error signals from the vibratory response of the smart foam itself. This can potentially improve the efficiency of the control algorithms and make way for a compact design of the smart foam system.

- **Control Strategy**

The final objective would be to establish the active control strategy that can be used with the transmission control application. The real-time control of optimizing the absorption coefficient of smart foams have been done using the fx-LMS algorithm. It remains to be seen if this methodology can perform with equal efficiency in the TL control application. Also, the use of alternate error sensors in the active control strategy may require a modification in the control algorithm which will also form a part of the present study. The efficiency of these active control algorithms has to be tested and optimized in real-time scenarios while minimizing the unwanted sound field.

1.1.3 Outline of the Thesis

The thesis is organized as follows. All the work has been compiled and put together in two articles which have been submitted to their respective journals (Journal of the Acoustical Society of America and Journal of Intelligent Material Systems and Structures). Here, the two articles have been reproduced in their entirety and contain the details of the methodology and results obtained during the course of the present research work.

The literature review on the application of smart foams in active noise control applications has been presented in section 1.1.1 which gives a background of the technological innovations that have been directed in this domain and helps to put the present work in context of the broader research perspective. The main objectives of the present masters research have been detailed in section 1.1.3.

Chapter 2 presents the first part of the thesis, which is in the form of an article that has been submitted to the Journal of the Acoustical Society of America. This part contains the details on the study of transmission loss with smart foams and the use of feedforward control to optimize the passive TL under broadband and tonal primary perturbation. The description of the finite element method used in the numerical simulations and the details of the physical noise control system has been presented in this work. The comparison of the simulation and experimental results throws significant light on the physical mechanism

of noise cancellation of the active noise control system, and the efficiency of the control mechanism along with the deviation of the physical system from the idealized simulation model has been studied in detail.

Chapter 3 contains the second part of this body of work and has been reproduced from a manuscript that has been submitted to the Journal of Intelligent Material Systems & Structures. It contains the details of the principle and methodology of implementation of a piezoelectric sensoriactuator that can be utilized as an error sensor in the active control technology in order to increase the compactness and efficiency of the noise control system compared to the use of far-field pressure sensors. The motivation of this innovation has been provided by the numerical simulations of the TL control problem which gives satisfactory improvement of the TL (in low and mid frequencies) under optimal control of the radial volume velocity of the continuous spatially distributed piezo-actuator embedded in the smart foam. Also, a virtual error control strategy has been realized with the piezoelectric sensoriactuators which helps to utilize the latter technology with both the absorption and transmission control problems. The results show satisfactory performance of this technique for both these optimization problems. However, some limitations in the performance of the control system over specific frequency bandwidths have been observed which have been reported in the article along with possible explanations for their under-performance.

Chapter 4 gives the general conclusions of the present work along with a summary of principal results that have been obtained from the finite element simulations and experimental active control studies. Based on these conclusions, the direction of future research in the domain of active noise control with smart foam technology, as foreseen by the author, has been enunciated briefly.

CHAPTER 2

Active Control of Transmission Loss with Smart Foams

Avant-propos

Authors :
A. Kundu : étudiant en maîtrise, Université de Sherbrooke, Faculté de génie, Département de génie mécanique.
A. Berry : professeur, Université de Sherbrooke, Faculté de génie, Département de génie mécanique.
Date of Submission : 24 March 2010
Journal : Journal of the Acoustical Society of America
Manuscript Number : MS 10-08786
Status : under review
Titre français : Contrôle actif de transmission loss à l'aide de mousses actives
Contribution of the document :
This paper presents the numerical simulation results of the transmission control problem along with the experimental study of the real-time feedforward control. The experimental results have been compared with the numerical simulation results and the mechanism of cancellation of the transmitted sound pressure is explained in light of the modification of the vibration response of the piezo-actuator of the smart foam. Thus the study forms an important and integral part of the present work and demonstrates applicability of the concept of smart foams to transmission control problems.
Résumé français :
Les mousses actives combinent les avantages complémentaires de matériaux en mousse passifs et d'un actionneur piézoélectrique spatialement distribué et intégré dans la mousse, pour des applications de contrôle actif du bruit. Dans ce document, le problème de l'amélioration de l'indice d'affaiblissement des mousses actives, en utilisant des stratégies de contrôle actif, a été étudié à la fois numériquement et expérimentalement. L'expérience s'est déroulée à l'intérieur d'un guide d'onde sous la condition de propagation en ondes planes. La simulation par éléments finis d'un système de contrôle de bruit couplé a été entreprise avec trois conceptions différentes de mousse active, et leur efficacité pour annuler

l'onde transmise en aval de la mousse active a été étudiée. Les résultats des simulations permettent de mieux comprendre le phénomène physique de l'annulation active du bruit et explique l'impact de la conception de mousse active sur les résultats du contrôle actif optimal. Des études expérimentales visant à mettre en œuvre le contrôle en temps réel pour l'optimisation de l'indice d'affaiblissement ont été effectuées en utilisant l'algorithme classique des moindres carrés. Les résultats de contrôle actif en large bande sous une source monofréquentielle démontrent une bonne amélioration de l'indice d'affaiblissement des mousses actives. L'étude donne une description comparative des problèmes de contrôle de la transmission et de l'absorption à la lumière de la modification de la réponse vibratoire de l'actionneur piézo-électrique sous contrôle actif.

2.1 Abstract

Smart foams combine the complementary advantages of passive foam material and spatially distributed piezoelectric actuator embedded in it for active noise control applications. In this paper, the problem of improving the transmission loss of smart foams using active control strategies has been investigated both numerically and experimentally inside a waveguide under the condition of plane wave propagation. The finite element simulation of a coupled noise control system has been undertaken with three different smart foam designs and their effectiveness in canceling the transmitted wave downstream of the smart foam has been studied. The simulation results provide insight into the physical phenomenon of active noise cancellation and explain the impact of the smart foam designs on the optimal active control results. Experimental studies aimed at implementing the real-time control for transmission loss optimization have been performed using the classical single input/single output filtered reference Least Mean Square algorithm. The active control results with broadband and single-frequency primary source inputs demonstrate a good improvement in the transmission loss of the smart foams. The study gives a comparative description of the transmission and absorption control problems in light of the modification of the vibration response of the piezoelectric actuator under active control.

2.2 Introduction

The smart foam advantageously combines the inherent mid to high frequency passive noise control capability of an acoustical foam treatment with the low frequency noise control capabilities of an active control system, and hence implementing the passive sound proofing

system as part of the active system to conserve weight and space [Guigou and Fuller, 1998]. Some of the hybrid passive-active approaches with foam materials for absorption control have been tested in the works of previous researchers using a strategy of imposing a *'zero pressure'* on the back of the porous material[Furstoss *et al.*, 1997; Galland *et al.*, 2005] or *'impedance matching'* of the active surface of the hybrid noise control system[Cobo *et al.*, 2003, 2004; Yuan, 2003]. They mostly used a secondary loudspeaker which acted as an active area behind a passive sound absorbent layer (e.g. micro-perforated absorbent, porous layer, etc.) with an error microphone, placed just behind the absorbent layer, to obtain the desired acoustic performance. Both these strategies, though effective in a broad frequency range, incurs a weight and space penalty that is undesirable in compact aerospace applications.

An alternate control strategy to this hybrid passive-active approach is offered by smart foams which integrate a distributed piezoelectric actuator into the passive sound absorbent material. The passive material performs satisfactorily at high frequencies in terms of attenuation of the incident noise, while the active actuator takes over in the low frequencies, where the efficiency of the passive layer is limited by the impractical space and weight requirements. The use of smart foams in acoustic radiation control problems has shown good noise control effectiveness over specified frequency bandwidths [Fuller *et al.*, 1996, 1994] in very thin and compact arrangements. Recent acoustic absorption control experiments undertaken with smart foams[Leroy *et al.*, 2009b; Leroy, 2008] show their effectiveness in enhancing the broadband absorption coefficient for normally incident plane waves. The acoustic transmission control problem with smart foams, however, still remains a sparsely studied domain, and is the prime focus of the current work.

The main objective of the current work is to enhance the acoustic Transmission Loss (TL) of a passive foam material using the smart foam principle, and to gain an in-depth understanding of the physical mechanism that leads to the above goal. In this paper the passive/active behavior of a smart foam is presented with the assumption of an acoustic plane wave incident normally on the smart foam, and it is partially transmitted to the other side of the smart foam. The smart foam design, in the present study, consists of a passive melamine foam material which is covered on its rear surface by a curved piezoelectric polyvinylidene fluoride (PVDF) membrane, which acts as the control actuator. The PVDF creates an acoustic insulation between the incident and transmitted sides of the smart foam, and this results in a high passive TL. For the case of active transmission control, the TL is enhanced further due to the vibration restructuring of the smart foam system,

and it results in a part of the incident acoustic energy being absorbed by the active PVDF membrane.

The outline of this paper is as follows. Sections 2.3.1 and 2.3.2 give a detailed description of the physical noise control system and the design of the smart foam prototypes used in the present study. Section 2.3.3 details the methods and equations used for evaluating the propagating wave components and the optimal control input. This is followed by the Finite Element simulation of the entire noise control system in Section 2.4. A complete finite element model of the poroelastic, piezoelectric, acoustic and elastic domains[Leroy *et al.*, 2009a] has been used to simulate the system response at each frequency for harmonic excitations of the primary and secondary sources. Section 2.4.1 includes the description of the modeling aspects of the smart foam prototypes and the noise control system as a whole, while section 2.4.2 gives a thorough description of the numerical simulation results. An in-depth analysis of the behavior of the noise control system is also presented here.

Following this, section 2.5 describes the experimental implementation of the real-time control of TL using digital signal processors. The TL control is implemented with single-input-single-output (SISO) adaptive feedforward controllers using the filtered-reference least mean square (Fx-LMS) algorithm with a unidirectional microphone providing the error signal. A brief description of the theory and methodology of feedforward control used for our noise control system is given in section 2.5.1. The behavior of the passive noise control system and the case of experimental active transmission control are detailed in section 2.5.2, along with the discussions related to the effectiveness and limitation of the control methodology.

2.3 Smart Foam and the Noise Control System : Description

2.3.1 Experimental Setup

The details of the smart foam and the physical noise control system used to implement the active TL control are described in this section. The smart foam is located inside a plexiglass cavity which has impedance tubes attached on both of its sides. The study is restricted the case of plane wave propagation in the impedance tubes.

The noise control system used in the present study is shown in Fig. 2.1. The incidence and transmission side impedance tubes on either side of the smart foam inside the plexiglass

cavity are shown in Figs. 2.1(a) and 2.1(b). The primary source comprises of two speakers placed face to face of each other at one end of the tube and perpendicular to the tube axis. Electret microphones, placed along the length of the impedance tubes, are utilized to evaluate the propagating wave amplitudes and hence record the efficiency of control. A complete description of the physical noise control set-up and the inter-microphone spacings on the incidence and transmission side waveguides are shown schematically in Fig. 2.1(c). The transmission side waveguide behind the plexiglass cavity ends in a rigid termination.

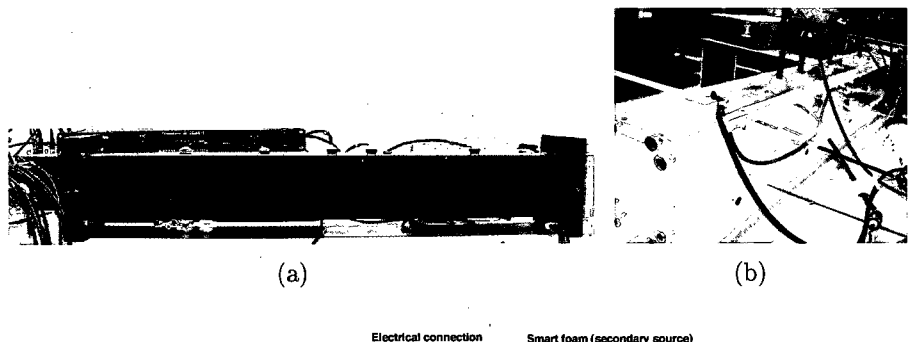

Figure 2.1 Physical Noise Control System with microphone positions along the length of the impedance tubes: (a) Absorption-side waveguide (b) Transmission-side waveguide (c) Schematic diagram of microphone positions in the waveguides

The different propagating wave components have been indicated in Fig. 2.1(c) which are evaluated with the help of microphone pairs using the classical two-microphone method [ASTM-E1050-98, 1998]. Also, a unidirectional electret microphone, which is utilized to provide the error signal for the implementation of real time control, is placed inside the transmission side waveguide at a distance of 45 cm from its right end rigid termination (shown later in Fig. 2.8). This microphone faces the smart foam and is used to detect the transmitted sound wave.

The high frequency limit of the problem is restricted to well below the higher mode cut-off frequency of the impedance tubes (which is roughly around 2200 Hz for our present case) to ensure plane wave propagation inside the tube. The different inter-microphone spacings ensure an accurate estimate of the propagating wave amplitudes at all frequencies (discussed in more detail in Section 2.5.1). It is ideally assumed that there is no other

acoustic transmission path between the incidence and transmission side waveguides other than through the smart foam. However, this assumption is not quite accurate for the actual physical noise control system assembly, as can be seen in the experimental results at low frequency.

2.3.2 Smart Foam Description

The smart foams used in our study are a composite noise control treatment consisting of a distributed PVDF actuator, attached on a layer of Melamine foam. Three different designs of smart foam with varying volume and actuator designs have been used in our study, as shown in Fig. 2.2(a) (refer to Table 2.1 for the geometric details of the individual prototypes). The first prototype, for example, is a half cylinder of foam with its curved rear surface covered with a PVDF film actuator. Since, melamine is highly porous, its surface is conditioned with a heat-reactivatable membrane and the PVDF is bonded onto it using a double-side tape. The bottom rectangular face of the smart foam is exposed to the normal plane acoustic waves.

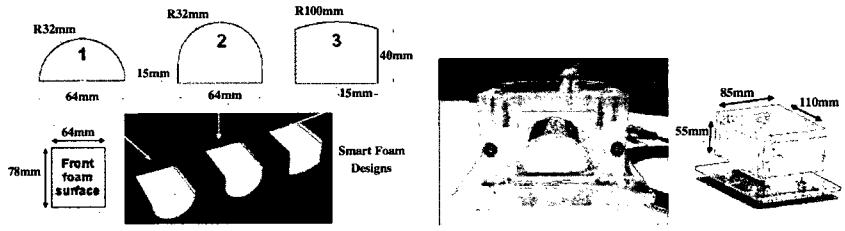

Figure 2.2 Smart Foams: (a) Designs of the 3 smart foam prototypes (b) Smart foam 1 inside plexiglass cavity

It is observed in subsequent sections that the different foam volumes and actuator designs of the three smart foam prototypes have a significant impact on the passive absorption and TL of the system. The varying PVDF film area and curvature markedly modify the sound radiation efficiency of the individual smart foams, and hence their control authority. The thickness of the PVDF membrane for all the three designs is 28 microns, and it possesses Cu-Ni surface electrodes. The smart foam system is mounted inside the plexiglass cavity equipped with electric connections which are used to drive the PVDF actuator, as shown in Fig. 2.2(b) (with the first prototype). Plexiglass flanges are placed on the lateral sides of the foam so as to ensure proper support conditions and tightness with the rear cavity.

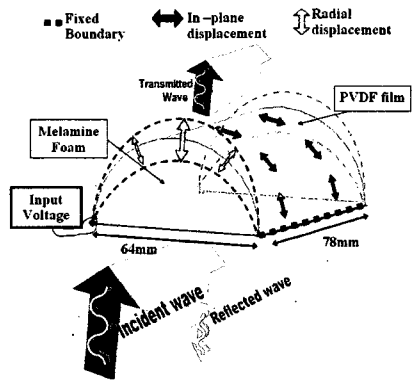

Figure 2.3 Action of smart foam

Fig. 2.3 shows the pumping action of the PVDF membrane of the first smart foam design, which is the fundamental mode of vibration of the PVDF in response to the acoustic waves and external electrical excitation. The curved shape of the PVDF membrane enables a strong coupling of the in-plane displacement components with the out-of-plane displacement. Since we assume an ideal condition of no acoustic leakage or flanking transmission paths between the incidence and transmission side waveguides, the transmitted sound pressure is solely a function of the vibro-acoustic response of the PVDF membrane, and the passive TL offered by the smart foams is quite high, especially at low frequencies. The absorption coefficient is also dependent on the vibration response of the PVDF membrane in addition to the passive dissipation in the foam material, which is seen in the numerical control results. Also, it should be mentioned that since the smart foams are placed inside the plexiglass cavity-waveguide assembly, its far-field radiation is significantly different from what it would have been in free field.

2.3.3 Absorption and Transmission Loss measurements

The complex propagating wave amplitudes have been derived using the Chung and Blaser method [Chung and Blaser, 1980], and the ASTM E1050 standard method [ASTM-E1050-98, 1998] with the several microphone pairs placed along the length of the tube and under the assumption of plane wave propagation. The different propagating wave amplitudes (incident $\widetilde{P}_1^-$, reflected $\widetilde{P}_1^+$, transmitted $\widetilde{P}_2^-$ and reflected-transmitted $\widetilde{P}_2^+$ as shown in Fig. 2.1(c)) are calculated using the classical expressions for plane wave components traveling in the positive z-direction, $\widetilde{P}^+$ (the reflected and reflected-transmitted wave amplitudes, Eq. (2.1a)) and negative z-direction, $\widetilde{P}^-$ (the incident and transmitted wave

amplitudes, Eq. (2.1b)) as follows :

$$\widetilde{P}^{+} = \frac{\widetilde{P}_n - \widetilde{P}_m e^{-ikd}}{2i\sin(kd)} e^{ikL_m}, \tag{2.1a}$$

$$\widetilde{P}^{-} = \frac{\widetilde{P}_n - \widetilde{P}_m e^{ikd}}{-2i\sin(kd)} e^{-ikL_m}. \tag{2.1b}$$

where the variables in Eqn. (2.1) are defined as follows: $\widetilde{P}_m$ and $\widetilde{P}_n$ are the complex values of pressure at the microphones placed at points m and n along the waveguide (maybe on either side of the smart foam) with point m situated further away from the origin in the positive z-direction than n, d is the distance between points m and n, k is the wavenumber and L_m is the distance of point m from the origin.

The 'offline' estimation of the optimal control input required to cancel a desired propagating pressure wave component is obtained utilizing the principle of superposition. Firstly, the system response under the action of the primary and secondary source inputs are evaluated separately. And then the optimal complex secondary source input, $\widetilde{\beta}^{+}$ or $\widetilde{\beta}^{-}$, required to cancel the reflected sound wave (propagating in the positive z-direction) or the transmitted sound waves (propagating in the negative z-direction) respectively, are calculated using the following expression :

$$\widetilde{\beta}^{\pm} = -\frac{\widetilde{H}p_{nm} - e^{\mp ikd}}{\widetilde{H}s_{nm} - e^{\mp ikd}} \tag{2.2}$$

where $\widetilde{H}p_{nm}$ and $\widetilde{H}s_{nm}$ are the transfer functions between microphone pairs under the action of the primary and secondary sources respectively and are expressed as $\widetilde{H}_{nm} = \frac{\widetilde{P}_n}{\widetilde{P}_m}$. The calculated $\widetilde{\beta}^{\pm}$ is a non-dimensional quantity which is normalized with the incident pressure amplitude to obtain the desired control voltage input per Pascal of the incident pressure. All these expressions are valid for the $e^{+i\omega t}$ time convention.

The acoustic energy indicators that have been monitored during the course of this optimization of control input are the absorption coefficient (α) and the Transmission Loss (TL) which are defined as in Eqns. 2.3:

$$\alpha = 1 - \left|\frac{\widetilde{P}_1^{+}}{\widetilde{P}_1^{-}}\right|^2, \tag{2.3a}$$

$$TL = 10log_{10}\left|\frac{\widetilde{P}_1^-}{\widetilde{P}_2^-}\right|^2. \tag{2.3b}$$

where $\widetilde{P}_1^-$, $\widetilde{P}_1^+$ and $\widetilde{P}_2^-$ are again the complex amplitudes of the propagating incident, reflected and transmitted pressure waves respectively. These energy indicators are key parameters in defining the performance of the noise control system and determining the efficiency of control.

2.4 Finite Element Simulation

This study comprises of a detailed finite element study of the response of the entire noise control system under primary and secondary source perturbations. We consider three different designs of the smart foam for the numerical simulations (as shown in Fig. 2.2(a)) and study their effectiveness in terms of the active and passive TL values and the actuator control authority. The simulations of the complete noise control system have been done with harmonic primary and secondary source disturbances introduced into the system over a bandwidth of 25 - 1500 Hz in steps of 25 Hz. The simulation gives the frequency domain response of all the degrees of freedom (*d.o.f.*) associated with each of node of the complete system. The amplitude and phase is obtained relative to the perturbation introduced into the system (either the primary source piston volume displacement, or the secondary source PVDF voltage input). These frequency domain data are utilized to calculate the acoustic energy indicators and the optimal control input required to minimize the desired propagating wave components.

2.4.1 The Finite Element Model

A 3-D finite element modeling of the complete noise control system shown in Fig. 2.1 (including acoustic, elastic, piezoelectric and poroelastic domains) is described here. It has been utilized in the present study to perform the numerical simulation of the entire noise control system. The finite element model for the poroelastic medium is based on an exact (u, p) formulation of the poroelastic domain [Atalla *et al.*, 2001; Debergue *et al.*, 1999]. The modeling utilizes quadratic poroelastic, elastic, fluid and piezoelectric elements to implement the weak integral formulation of these different media involved in the problem along with the associated coupling and boundary conditions [Leroy *et al.*, 2009a; Leroy, 2008]. The individual elements involved in the modeling of the system are as follows :

1. The poroelastic domain for the foam material has been modeled with 20 noded brick elements based on an orthotropic definition of the solid phase, and they have

4 degrees of freedom associated with each node : 3 orthogonal translations and 1 pressure, which results in 80 degrees of freedom per element.

2. The acoustic domain comprises of the 20 noded classical fluid elements with one degree of freedom (pressure) per node.
3. We have used two kinds of elastic elements in the model viz (*i*) 20-noded classical brick elements with 3 translational degrees of freedom per node to model the 3-dimensional waveguide terminations on the left and right of the incidence and transmission side impedance tubes respectively, so as to suppress their modal vibrations, restricting them to execute rigid body motion only, and (*ii*) 8-noded plate elements with 6 degrees of freedom per node (3 translations and 3 rotations) to model the elastic bonding layer between the poroelastic foam and the piezoelectric domain.
4. Surface piezoelectric elements comprising of 8 nodes with 7 degrees of freedom per node (3 translations, 3 rotations and 1 electrical potential) to model the PVDF actuator.
5. Lastly, the fluid-structure coupling [Debergue *et al.*, 1999] was implemented with 8-noded surface elements to account for the acoustic-poroelastic, acoustic-piezoelectric, poroelastic-piezoelectric and acoustic-elastic interface conditions.

We have used two different boundary conditions in our model : (*i*) fixed displacement and (*ii*) fixed electrical potential to introduce forcing terms into the system. The primary loudspeaker has been modeled with a fixed harmonic displacement imposed on all the nodes of the left waveguide termination on Fig. 2.1(c) over the entire frequency range, while the electrical excitation imposed on the PVDF membrane has been modeled with a fixed harmonic electric potential imposed on the piezoelectric domain. The boundary conditions imposed on the PVDF membrane are of particular importance to the radiation efficiency of the smart foams, since they significantly modify the relative structural modal contributions in its vibration response. The curved edges of the PVDF membrane have all their nodal translational d.o.f. blocked while the straight edges (coinciding with the two opposite rectangular edges of the bottom surface of the foam as in Fig. 2.3) have all (both their translational and rotational) d.o.f. fixed to zero. The acoustic domain is assumed to be inside a perfectly rigid structure (the impedance tube and the plexiglass cavity) and therefore, the acoustic pressure gradient normal to the rigid walls has been set to zero. There is no pressure continuity between the acoustic elements on the incident and transmission sides of the waveguide, thus the transmitted sound pressure is solely a function of the vibratory response of the PVDF membrane which forms an impervious membrane on the rear side of the foam surface.

Previous measurement of the elastic and acoustic properties of the melamine foam has revealed that the foam material is anisotropic [Leroy *et al.*, 2009b]. However, for the present case of numerical simulations, the anisotropic effects are considered for the elastic parameters only, while the acoustical parameters are taken to behave isotropically. The property values of the melamine foam are listed in Table 2.2. The elastic and piezoelectric property values of the PVDF membrane have been incorporated from published data [Bailo *et al.*, 2003] (Table 2.3). It is to be noted that the higher of the two piezoelectric strain constants i.e. e_{32} has been used along the circumferential direction of the PVDF membrane to facilitate a larger electromechanical coupling along this direction, which helps in enhanced vibration response and radiation efficiency of the PVDF actuator per unit input of the electrical voltage. The material property values of the elastic bonding material between the PVDF membrane and the passive foam material that has been used in the simulations are listed in Table 2.4 (using published data [Leroy *et al.*, 2009a]). The finite element model assumes no acoustical leakage or flanking paths between the incidence and transmission sides of the smart foam across the plexiglass cavity.

The extremely small thickness of the PVDF membrane could have led to enormous calculation time and memory requirements, however, in light of the added stiffness of the bonding layer and the foam, a manageable element size of has been found to be acceptable according to convergence analysis. Higher mesh density is used in the acoustic domain in proximity to the smart foam in order to capture the effects of the higher order evanescent waves (the acoustic near field).

2.4.2 Simulation Results

Active noise control simulations with the different smart foam prototypes are presented here. The frequency response of the entire system is evaluated at each frequency from 25 to 1500 Hz (in steps of 25 Hz) and optimal control is performed using the transmitted pressure amplitude as the minimization criterion. Under the action of the primary source, the acoustic pressure amplitudes and the energy indicator plots are shown in Fig. (2.4) and a number of observations can be made from the curves. The peaks in the wave amplitude curves correspond to the longitudinal acoustic standing wave resonance frequencies along the length of the impedance tubes on the incidence and transmission sides of the smart foam. Since the lengths of the two impedance tubes are different, the peaks in the transmitted wave amplitude are due to the standing waves both on the incidence and transmission sides of the smart foam.

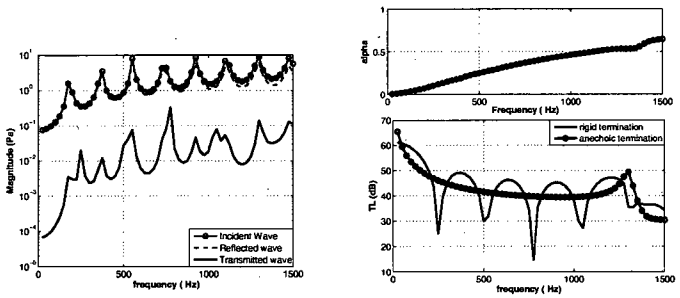

(a) (b)

Figure 2.4 Response of the noise control system with design 1 of the smart foam under the action of primary source: (a) Amplitude of Incident, Reflected & Transmitted Pressure waves (b) Absorption coefficient (top) and Transmission Loss (bottom)

The absorption coefficient (Fig. 2.4(b)) is found to increase with frequency, which is mainly due to the enhanced passive dissipation in the foam material. The high value of passive transmission loss, especially at low frequencies, as seen in Fig. 2.4(b), is mostly due to the impervious and comparatively rigid membrane formed by the PVDF film, whose side edges are pinned. This figure gives the TL of the system both with a rigid and an anechoic termination of the transmission-side waveguide (for details of the numerical implementation of the anechoic termination, see Ref. [Kundu *et al.*, 2009]). The effect of the transmission side standing waves are clear at the frequencies where the rigid-termination TL (in Fig. 2.4(b)) decreases sharply. However, by implementing the anechoic termination, we eliminate the possibility of formation of standing waves on the transmission side, and thus obtain a more uniform TL curve, which provides a better estimation of the fraction of incident acoustic energy transmitted through the smart foam.

The optimal control results for the three smart foams of Fig. 2.2(a) are shown in Fig. 2.5. The magnitude of the transmitted wave for optimal control is derived using the two microphone method (described in Section 2.3.3) and using the expressions given in Eqns. 2.1 and 3.1. Figs. 2.5(a), 2.5(b) and 2.5(c) show the control effort per unit incident pressure (in Pascal) required to cancel the transmitted pressure wave. The phase of the control input for transmission control has been calculated with respect to the net fluid particle velocity on the foam surface (plotted with continuous lines). It is worth pointing out that the control input required to obtain a complete cancelation of the transmitted pressure wave is independent of a rigid or an anechoic termination of the transmission-side waveguide [Kundu *et al.*, 2009]. Here, a comparison of the control input phase response of the transmission control problem has been made with that of the absorption control prob-

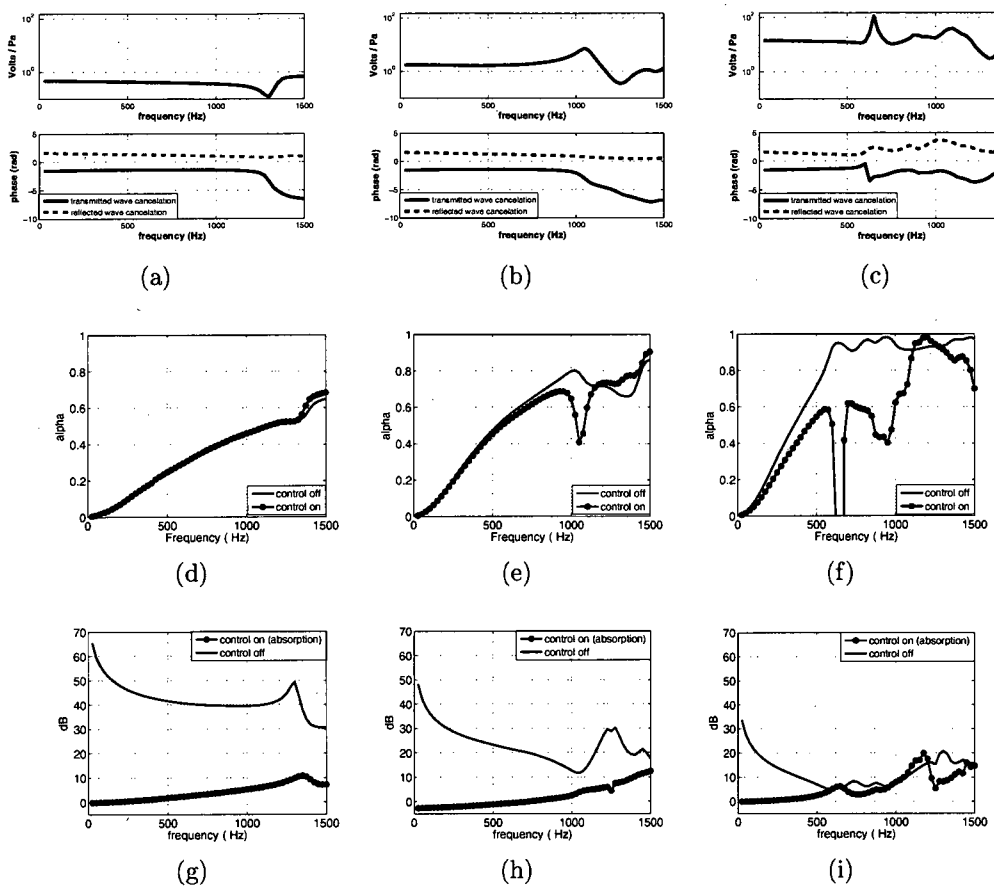

Figure 2.5 Optimal active control simulations for the smart foam designs 1, 2 and 3 (left, center and right respectively): (a), (b), (c) show the amplitude and phase of the control input for transmitted wave cancelation; (d), (e), (f) show the absorption coefficient for the case of cancelation of transmitted wave (transmission control); (g), (h), (i) show the TL for the case of cancelation of reflected wave (absorption control).

lem (the absorption control problem basically deals with the cancelation of the reflected pressure wave from the foam surface and hence enhance the total acoustic absorption by the smart foam). It is seen that there is a phase difference of approximately 180^o in the actuator inputs between the absorption and transmission control problem, especially at low frequencies. Now, a 90^o phase difference of the control input with the net fluid particle velocity on the foam surface (which is the case for the absorption control problem at low and mid-frequencies) implies that the displacement of the PVDF membrane is in phase with the fluid particle displacement on the foam surface. Hence a -90^o phase angle of the control input (at low and mid-frequencies for the transmission control problem) would imply out-of-phase motion of the PVDF membrane with respect to the foam surface fluid

particle velocity. This shows that the mechanism of cancelation of the transmitted wave is to create a secondary volume velocity opposite in phase to the volume velocity of the incident wave, whereas the mechanism of cancelation of the reflected wave is to create a perfect impedance matching condition at the secondary source position.

A further careful observation reveals that the control input phase angle for the absorption problem slowly decreases from 90^o with frequency with respect to the acoustic particle velocity on the foam surface (especially for the first two designs), which can be attributed to the propagation delay associated with the passive foam material. However, the TL control phase response is found to be constant at low and mid-frequencies (again for the first two designs). This is explained as follows: the mechanism of cancelation of the transmitted pressure, at least in the low and mid-frequencies (when the fundamental or the breathing mode of the PVDF is most significant), is concerned with stalling the motion of the PVDF membrane entirely, so that there is practically no acoustic radiation (near or far-field) from the actuator surface on the transmission side of the smart foam. Thus, the control effort is almost in a constant phase relation relative to the particle velocity on the foam surface. The effect of propagation delay found for active absorption control, where the PVDF radiation is enhanced in order to create a perfect impedance match for the incident acoustic wave, is not observed for TL control. It can be seen in Figs. 2.5(g), 2.5(h) and 2.5(i) that the absorption control problem results in an appreciable decrease on the TL values.

However, at higher frequencies (beyond approximately 1200 Hz for design 1) the phase response for all the three designs of smart foam tend to become more complicated. It can be intuitively put forward that, beyond this frequency, the (3,1) mode shape of the PVDF membrane becomes more significant, and hence TL enhancement no longer takes place via stalling the PVDF motion. Instead, the actuator vibration response is modified in such a manner so as to cancel the net far-field acoustic pressure on the transmission side of the smart foam. However, this does not ensure a zero near field pressure.

This is verified from observing Fig. 2.6 which gives the spatial distribution of the squared acoustic pressure derived from the Finite Element simulation in the near-field and inside the waveguide behind the smart foam. Fig. 2.6(a) shows the acoustic pressure field under the action of the primary source at 1500 Hz (note that this is a sectional view of the transmission side waveguide behind the smart foam, and only the acoustic domain is presented in the figure for the sake of clarity). The high squared pressure in the waveguide before control (Fig. 2.6(a)) is due to the propagating transmitted wave (note again that the waveguide has an anechoic termination, and thus no standing waves). Fig. 2.6(b) shows the

situation under active transmission control, and it demonstrates that although we have a practically zero acoustic pressure in the waveguide, i.e. no propagating transmitted acoustic pressure, there is a significant acoustic near-field that exists inside the plexiglass cavity behind the smart foam. A comparison of the near field acoustic pressure before

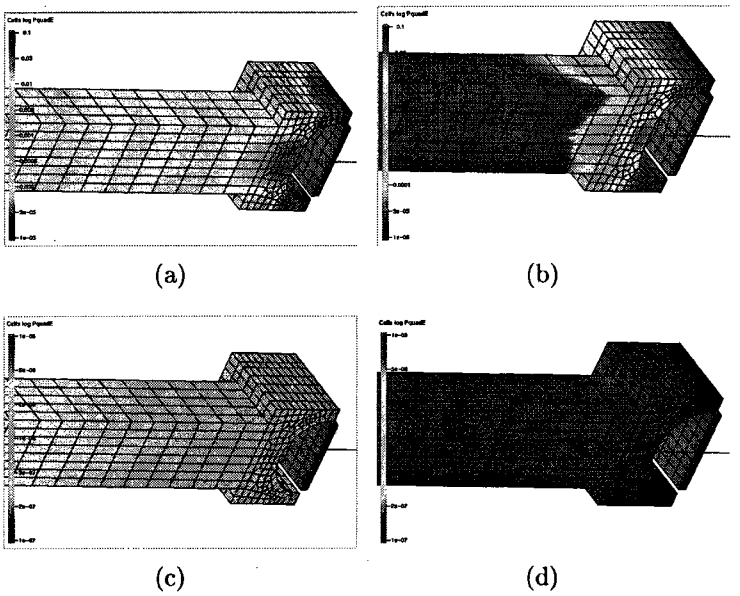

Figure 2.6 ("Color online") Squared acoustic pressure field behind the smart foam before and after cancelation of transmitted pressure: (a) Before Control at 1500 Hz (b) After Control at 1500 Hz (c) Before Control at 300 Hz (d) After Control at 300 Hz

and after control at 300 Hz is given in Figs. 2.6(c) and 2.6(d) respectively, and it shows a complete acoustic isolation of the transmission side of the smart foam from the incidence side under control. This indicates a complete stalling of the PVDF motion under control at 300 Hz. Thus, at higher frequencies, the TL control is not concerned with the minimization of radiation from the PVDF surface, rather it aims at vibration restructuring of the PVDF membrane order to cancel the far-field pressure in the transmission side waveguide.

A careful observation of the control inputs in Figs. 2.5(b) and 2.5(c) clearly shows a peak in the control effort for the the second and third designs at 1050 Hz and 650 Hz respectively. This can be justifiably interpreted as the enhanced control input required to control the resonance response of the fundamental vibratory modes of these smart-foam designs. Also, since the third smart foam prototype is bulkier that the second prototype, its fundamental structural resonance frequency is understandably lower. This can also be seen in the absorption coefficient curves under TL control in Figs. 2.5(e) and 2.5(f). At the particular above mentioned frequencies, the absorption coefficients of the second and

third designs are found to decrease abruptly compared to their passive values which can be interpreted as follows: the control input at these resonance frequencies tends to completely restrict the motion of the PVDF membrane and hence the foam layers adjacent to it. This leads to appreciably lower dissipation of the incident acoustic energy in the poroelastic domain. Thus a large portion of the acoustical energy is reflected back from the smart foam surface resulting in low values of absorption coefficient. The first design however, is not found to exhibit this kind of particularly sharp resonance behavior, although we find an increase in the transmission control input around 1300 Hz in Fig.2.5(a). Also, the first design, being less bulky than the other two designs, is expected to have a higher resonance frequency.

It should also be pointed out, however, that the far-field acoustic radiation in the waveguide is significantly altered by the presence of the complex geometry of the plexiglass cavity and the abrupt change in cross-section at the (transmitted-side) waveguide-plexiglass cavity interface. The behavior of the smart foam can be expected to be significantly different in free-field conditions, and hence the control input and vibration restructuring of the PVDF membrane (especially at mid and high frequencies) to produce a zero transmitted wave would depend on the position of the error sensors, and would be significantly different for local and global control strategies.

The theoretical transmission loss obtained under control, tends to infinity, which indicates the ideal situation where the transmitted sound wave has been completely canceled. Figs. 2.5(d), 2.5(e) and 2.5(f) show the absorption coefficient results in control 'off' and 'on' states, and they indicate that for the first design of the smart foam, the absorption coefficient practically remains unchanged under TL control. This indicates that the absorption and transmission control problems are appreciably decoupled for this design. However, the problems are quite coupled for the other two designs, particularly for the third one.

Also, for the case of absorption control simulations (for details, see Ref. [Kundu *et al.*, 2009]), the TL values under control decreases significantly for all the three designs, at least in the low and mid frequencies. This indicates that the action of the PVDF under absorption control enhances the transparency of the smart foam to the incident acoustic energy, as can be seen in Figs. 2.5(g), 2.5(h) and 2.5(i). It should be noted that the TL curves, shown here have been obtained for an anechoic termination implemented on the transmission side waveguide (compare with Fig. 2.4(b)). The third design exhibits the highest passive absorption coefficient (Fig. 2.5(f)), and also the lowest value of passive TL (as in Fig. 2.5(i)) under the action of the primary source only. Thus the transmitted

pressure under passive operating condition is larger for this design, especially when the absorption coefficient is close to 1.

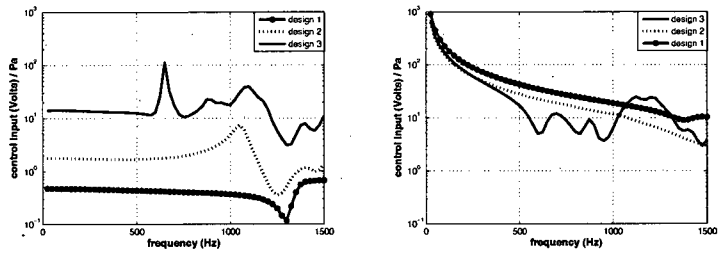

(a) (b)

Figure 2.7 Comparison of Control Input per unit incident acoustic pressure on the foam surface: (a) Cancelation of transmitted wave (b) Cancelation of the reflected wave

This provides us with a fairly clear understanding of the actual energy balance taking place in the noise control system. The modification of the PVDF actuator response under transmission control, enhances the reflected pressure amplitude which results in an appreciable decrease in the absorption coefficient under control, especially at mid and high frequencies for the second and third designs. However, the effect is almost negligible for design 1 which has a high passive TL. Hence the control input required to cancel the transmitted wave is quite less to appreciably modify the absorption coefficient for this design, as in Fig. 2.5(d).

This conclusively indicates that the high value of passive absorption coefficient for the third design, owes a lot to the particular geometrical shape and area of the PVDF membrane (refer to Fig. 2.2(a)), which makes it a better vibroacoustic radiator compared to the first two designs. Thus, it can be said, in general that for comparable volumes of the passive foam material contained in the smart foam designs, for instance the second and third designs in our case (refer to Table 2.1 for geometrical details of the individual prototypes), a higher radiation efficiency of the PVDF membrane would translate into a better absorption coefficient and a poor TL for that design under passive operating conditions. This fairly clear understanding of the vibration response of the PVDF actuator and its effect on the pressure field inside the waveguide can present us with alternative sensing strategies (to far-field directional microphones that are being used currently) to cancel the propagating pressure wave components. The PVDF sensori-actuator can be one of the approaches that might prove effective.

A comparison of the control inputs required for transmission and absorption control problem (Fig. 2.7) shows opposite trends in terms of the control authority required. Design 1 requires the smallest control input magnitude for the transmission control problem, while it is design 3 for the absorption control problem (at least up to 1000 Hz, which can be held satisfactory, since beyond that frequency, the passive absorption coefficient itself is quite close to 1). However, the comparatively lower value of the transmission control effort for design 1 reflects the fact that the amplitude of the transmitted pressure wave is much lower than that for the other two designs, mainly due to the particular design of PVDF membrane, which renders it to be a poor vibroacoustic radiator.

2.5 Active Transmission Control Experiments

The TL performance of the smart foam, which has been described in detail in section 2.3, is presented here, along with the real-time implementation of the control of transmitted wave. The idealized assumptions made in the numerical simulations regarding the material properties, transmission paths and linearity of the smart foam system however, do not hold strictly for the actual test setup. The frequency range of interest in the present case is 100 - 1500 Hz, which is below the cut-off frequency of the waveguide for plane wave propagation. Active control has been performed with broadband and tonal disturbances over this frequency range. Feedforward time domain adaptive controllers have been used for all the cases. For the sake of conciseness, the control results presented here have been limited to the first design of the smart foam only.

2.5.1 Feedforward Control

Real time feedforward control, which requires the use of a reference signal, has been used to enhance the TL of the smart foam. We have used an adaptive[Widrow and Stearns, 1985] SISO (single input single output) linear fx-LMS control algorithm and a block diagram of this is shown in Fig. 2.8, along with a sketch of the associated physical noise control system with the respective sources and microphone sensors. The signal acquisition and online implementation of the feedforward control algorithm is performed using a dSPACE platform, which is fast enough to implement zero wait state operation of the signal analyzer. The control algorithm is programmed in Matlab-Simulink and implemented into the signal processor hardware. The digital sampling frequency is set to 4 kHz. All the analog components are connected to the signal analyzer board through anti-aliasing filters and the sampled digital signal outputs are passed through reconstruction filters. Both the

anti-aliasing and the reconstruction filters, used in the present study, are low-pass hybrid analog-digital filters (Musilab: FPB25), and they have an almost flat frequency response in the passband below the Nyquist frequency (2 kHz) of the present problem. The reference signal is obtained from the input to the primary source. The primary input is amplified using a Sony TA-N220 Power Amplifier and fed into the loudspeakers on the left end of the absorption side waveguide. The error signal is provided by the unidirectional microphone that is placed inside the transmission side waveguide, and it is a cardioid Panasonic electret cartridge (WM-55A103) with a relatively flat relative response of 15dB between the 0^o and 180^o directions from 400-3000 Hz. The relative response, however, falls rapidly below 400 Hz, making the cartridge an almost omnidirectional microphone at low frequency. The secondary source input is fed to the PVDF membrane after passing it through a linear topology amplifier (PCB Piezotronics - AVC 790 Series), with a maximum voltage limit of 200 Volts.

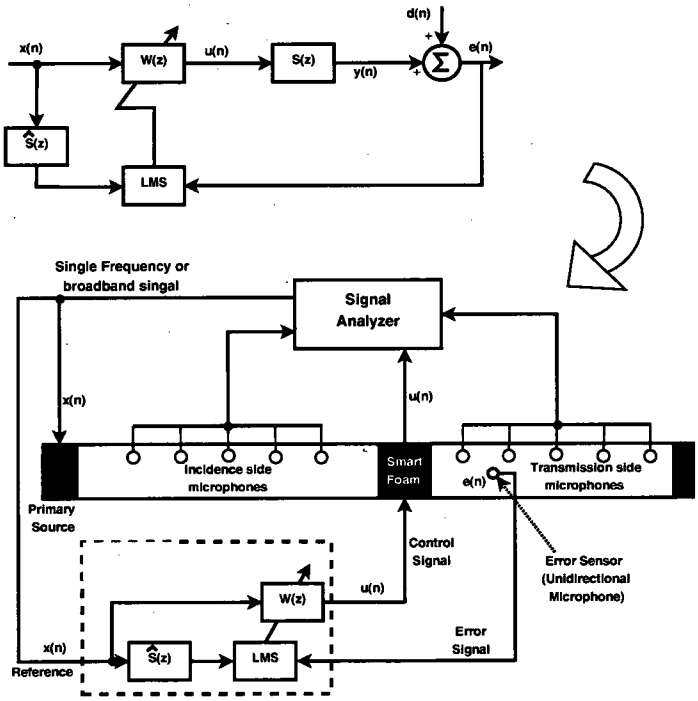

Figure 2.8 Block diagram of Adaptive Feedforward Control and a Schematic Diagram of the Experimental Active Control System

The microphones placed along the length of the waveguides are used to monitor the propagative wave magnitudes on both sides of the smart foam and the inter-microphone spacings have been chosen so as to have a satisfactory accuracy in the measurement of the propagating wave amplitudes (using the two microphone method [Chung and Blaser,

1980]). The phase difference between two microphones has to be at least 7^o for accurate measurement, which translates into a minimum spacing of 7 cm at the lowest frequency of 100 Hz. The high frequency limit restriction on the microphone spacing (d) can be defined by the requirement of $d < m\lambda/2$ where m is any non-zero integer, and λ is the acoustic wavelength at that frequency. Taking $m = 1$, we must have a maximum microphone spacing of less than 11 cm at 1500 Hz. These constraints have been maintained in the choice of the inter-microphone spacings on the incidence and transmission side waveguides. Thus, the pair $1 - 2$ (with maximum spacing) is suitable for low frequency measurements, while pair $3 - 4$ (with minimum spacing) is ideal at the high frequencies. The calculated pressure amplitudes, using these different microphone pairs, are utilized to determine the control effectiveness and evaluate the acoustic energy indicators before and after the implementation of the real-time control.

Fig. 2.8 shows the secondary path transfer function $S(z)$ (which is the transfer function between electrical input to the PVDF actuator and the error microphone output) is identified offline as a Finite Impulse Response (FIR) filter and its estimate, denoted by $\hat{S}(z)$, is used to filter the reference signal to modify the FIR control filter coefficients using the stochastic gradient algorithm. It is necessary to have a reference signal, $x(n)$, having a good coherence with the error signal $e(n)$, in order to generate the appropriate control input $u(n)$. The reference signal is filtered through an adaptive FIR control filter $\mathbf{W} = [w_0 \ ... \ w_{J-1}]^T$ having J-coefficients and is used to drive the PVDF actuator to minimize the error signal. The update equation of the control filter weights in the stochastic gradient algorithm is :

$$w_j(n+1) = w_j(n) + 2\mu x^{'}(n-j)e(n) \tag{2.4}$$

Here n is the discrete time step, $x^{'}(n) = [s_0 \ ... \ s_{I-1}] \times [x(n) \ ... \ x(n-I+1)]^T$ is the reference signal filtered by the I-coefficients of the identified secondary path $\hat{S}(z)$ and μ is a convergence parameter that controls the stability and the convergence of the update equation.

The identification of the plant response $\hat{S}$ for the broadband active control has been performed with $I = 300$ coefficients while the number of coefficients of the control filter $\mathbf{W}$, is $J = 350$. The identified plant model and the control filters (which are obtained using the gradient algorithm) can be compared with the estimates obtained from optimal

frequency domain expressions [Elliott, 2001] following Eqs. 2.5 and 2.6,

$$\hat{S}(e^{j\omega T}) = \frac{S_{ye}(e^{j\omega T})}{S_{yy}(e^{j\omega T})}, \tag{2.5}$$

$$W(e^{j\omega T}) = -\frac{S_{xd}(e^{j\omega T})}{\hat{S}(e^{j\omega T})S_{xx}(e^{j\omega T})}, \tag{2.6}$$

where S_{ye} is the cross spectral density between the secondary source input and the error microphone response under the action of the secondary source only and S_{yy} is the power spectral density of the secondary source input. Similarly, S_{xd} is the cross spectral density between the primary input and the error microphone response, and S_{xx} is the power spectral density of the primary input. Note that Eqs. 2.5 and 2.6 do not guarantee the causality of the controller. Active control of single frequency primary disturbance, however, requires fewer number of control filter coefficients than the broadband problem (theoretically only two coefficients would be sufficient to determine the appropriate amplitude and phase of the control input). For the present problem though, 50 control coefficients have been used to ensure a stable performance.

The causality constraint requires that the delay involved in the primary propagation path is larger than the total delay involved in the control filter and the secondary path. The anticipation time, which is the difference between the primary and secondary propagation paths, can significantly alter the performance of the system. It has been seen in previous studies of absorption control that, introducing an artificial added delay in the primary path can result in improved performance [Leroy *et al.*, 2009b]. However, the present study has not attempted to artificially introducing any delay in the primary path to improve the control results.

2.5.2 Experimental Results

System Response under the action of primary and secondary source

The response of the system under the action of the primary source is presented in Fig. 2.9. The acoustic pressure magnitudes of the propagating waves for a broadband input of the primary loudspeaker, as extracted with the microphone pairs, show the standing wave frequencies on the incident and transmission sides of the impedance tube (Fig. 2.9(a)). Due to a high passive transmission loss offered by this first design of the smart foam the magnitude of the transmitted wave decreases appreciably beyond 800 Hz; hence, the signal to noise ratio decreases appreciably on the transmission side beyond this frequency.

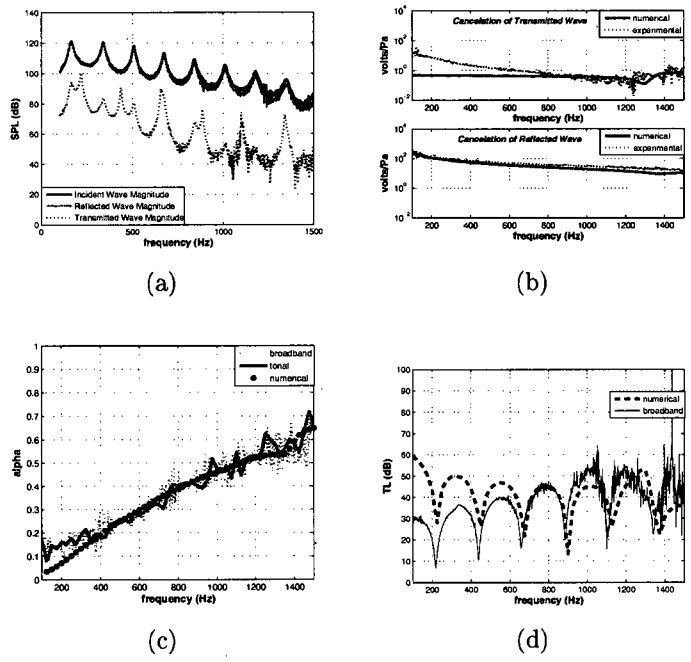

Figure 2.9 System response under the action of the primary and secondary sources: (a) Magnitude of propagative wave components for broadband input of the primary loudspeaker (b) Optimal control input magnitudes for cancelation of transmitted and reflected waves, per unit magnitude of the incident wave (c) Absorption coefficient (d) Transmission Loss

The comparisons of absorption coefficient and TL under tonal and broadband primary source input with numerical simulations are shown in Figs. 2.9(c) and 2.9(d) respectively. The finite element model provides a fairly accurate prediction of the absorption coefficient except at low frequencies (below 400 Hz), where the experimental results indicate a smaller reflected wave from the foam surface. The TL results show that the numerical model significantly overestimates the actual TL obtained in the experiments at low frequency. This can be attributed to the fact that, at low frequency the structure-borne noise carried by walls of the waveguide and walls of the smart foam cell creates a significant flanking transmission path, which modifies the transmitted sound pressure values. Also, the assumption of a completely leak-proof smart foam-plexiglass flange arrangement in case of the numerical simulations does not hold strictly for the experimental setup, due to imperfections in the system assembly.

Fig. 2.9(b) shows the control efforts required for cancelation of reflected and transmitted waves. They have been evaluated 'offline' (using Eq. 3.1), based on the measured propagating wave amplitudes, and have been compared with the finite element results. Again,

it can be seen that there is a fairly good agreement of the experimental results with the numerical simulations. However, at low frequencies, the TL control results show that the numerical simulation has under-estimated the required control input. This can again be explained in light of the lower TL value found in the experimental results, which implies a higher transmitted wave amplitude, and hence an enhanced control input to cancel the same, in the low and mid frequency range. Also, due to a large passive TL of the smart foam, the optimal control input is generally much lower for cancelation of the transmitted wave than that for the cancelation of reflected wave from the foam surface.

Active Control Results

Active control experiments have been performed using the classical fx-LMS algorithm, which involves the identification of the plant model. In the control situation, the reference signal is filtered by this plant model for determining and updating of the control coefficients in real-time. Fig. 2.10(a) shows the frequency domain response of the control filter obtained after convergence of the control filter (for broadband primary disturbance), and it has been compared with the causally unconstrained optimal frequency response based on the error microphone readings under the primary and secondary source inputs, using Eqs. (2.5) and (2.6). The frequency response of the control filter is thus the required control effort, in

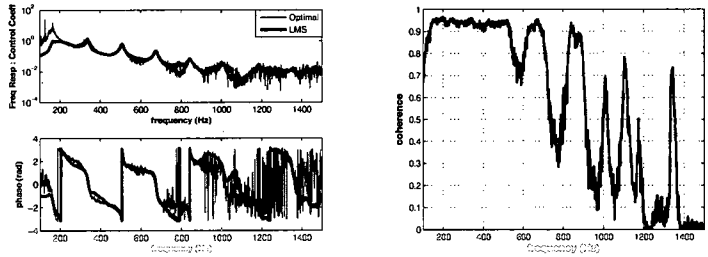

(a) (b)

Figure 2.10 Control Filter: (a) Frequency response of the control filter (b) Coherence between primary source input and error microphone

amplitude and phase, per unit input of the primary source. Also, the fact that the causally unconstrained frequency response is close to the actual frequency response of the control filter demonstrates that causality does not pose any significant problem in the present case. It is also seen that the optimal frequency response of the control filters is quite noisy beyond 800 Hz which can be attributed to the poor signal to noise ratio at the error microphone under passive operating conditions, as can be verified from the significant drop in coherence between the primary source input and the error microphone beyond 800 Hz in Fig. 2.10(b).

Fig. 2.11 shows that excellent reductions in the transmitted pressure amplitude has been obtained in the low and mid frequency range accompanied by a significant increase in TL before and after control for broadband primary disturbance. The transmitted pressure amplitude shown in Fig. 2.11(a) has been normalized with the primary source input. Fig.2.11(b) shows the improvement in TL values under control. However, a poor signal to noise ratio beyond 800 Hz leads to a deterioration in control effectiveness in the frequency range of 800 - 1500 Hz.

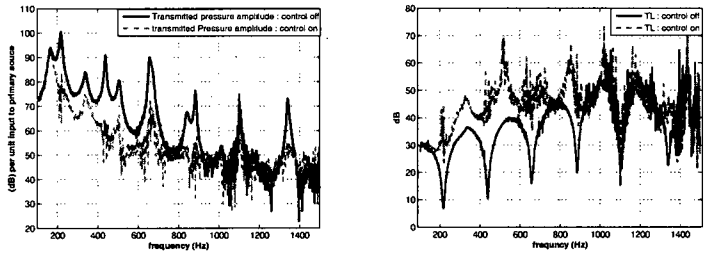

(a) (b)

Figure 2.11 Active control of transmitted wave magnitude for broadband disturbance: (a) Magnitude of transmitted wave (b) Transmission Loss

The experiment has been repeated with single frequency harmonic inputs as primary disturbances and the system response under these perturbations are as given in Fig. 2.12. The active control input (in volts per Pascal of the incident wave amplitude) to the PVDF

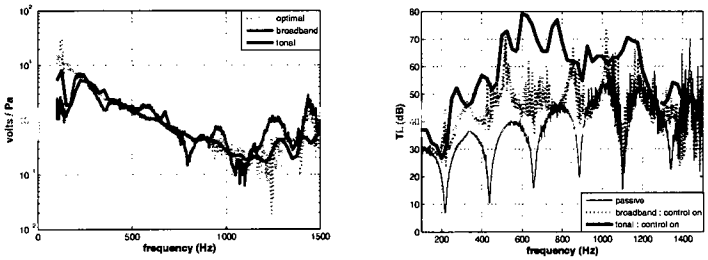

(a) (b)

Figure 2.12 Active control results for broadband and single frequency input: (a) Control input per unit incident wave magnitude (b) Transmission Loss

actuator required to minimize the transmitted wave amplitude is shown in Fig. 2.12(a). We find a fair agreement of these control efforts under the action of broadband (100 - 1500 Hz) and single frequency primary inputs and they have been compared with the optimal values derived from offline measurements of the primary and secondary waves. The tonal control is found to produce much better TL control results compared to that of

broadband noise control, as can be seen in Fig. 2.12(b). The large decrease in the passive TL associated to standing wave resonances on the transmission side of the waveguide has been satisfactorily eliminated under active control. This is because, at the resonance frequencies of the acoustic modes in the waveguide, the sound field is dominated by a single modal contribution which is satisfactorily attenuated by the secondary source.

The deterioration of the TL control in the high frequency range for the case of broadband noise can be primarily attributed to the following two reasons. Firstly, a poor signal to noise ratio at the error microphone at the high frequencies, especially between resonance points, for broadband primary input leads to deterioration of the control performance. Secondly, it must be pointed out that the non-linearity of the PVDF actuator and the bonding material has the potential to contribute to the deterioration of the control effectiveness especially at high frequencies, when the amplitude of the higher structural modes of vibration of the PVDF actuator is expected to be more pronounced.

2.6 Conclusion

This study proves the applicability and effectiveness of the smart foam concept to increase the transmission loss of a passive treatment. The experiments conducted in a waveguide under the assumption of plane wave propagation demonstrate a satisfactory improvement in the passive TL value under the action of single frequency harmonic disturbance and broadband noise.

Thus, the following important points can be summarized at the conclusion of the present study:

- The Finite Element model adequately predicts the sound absorption and transmission phenomena through the smart foam;
- The TL overestimation in the numerical simulation is primarily due to the presence of significant flanking transmission path in the experimental setup, which was not taken into account in the numerical simulations;
- Significant TL improvement have been obtained under single-frequency and broadband disturbances up to 800 Hz;
- Above 800 Hz, the poor control result with broadband noise can be attributed to very low level of passively transmitted noise and possibly non-linear response of the smart foam;
- In cancelation of transmitted wave, the active control mechanism is concerned with the vibration reduction of the PVDF membrane in low frequency, and vibration restructuring in higher frequency;

Future work along this direction may concentrate on investigating alternate sources of deriving the error signal, which can lead to further control effectiveness and compactness of the active control system.

Acknowledgments

The authors would like to acknowledge the support of the Natural Sciences and Engineering Research Council of Canada, Bombardier Aerospace, Pratt & Whitney Canada and Bell Helicopter Textron Canada.

Table 2.1 Geometrical Parameters of the Smart Foam prototypes.

Parameters	*Smart Foam* 1	*Smart Foam* 2	*Smart Foam* 3
Foam volume (cm^3)	125	200	225
Mean Thickness (cm)	2.5	4	4.4
PVDF area (cm^2)	78	101	115

Table 2.2 Structural and acoustical parameters of the melamine foam.

Parameters	*Name*	*Value*	*Unit*
ϕ	Porosity	0.96	-
σ	Resistivity	1.53×10^{-4}	$N.s.m^{-4}$
α_∞	Tortuosity	1.02	-
Λ	Viscous characteristic length	105×10^{-6}	m
Λ'	Thermal characteristic length	205×10^{-6}	m
ρ	Mass density	9	$kg.m^{-3}$
E_x	Young's modulus(x dir.)	4.0×10^5	$N.m^{-2}$
E_y	Young's modulus(y dir.)	1.8×10^5	$N.m^{-2}$
E_z	Young's modulus(z dir.)	0.55×10^5	$N.m^{-2}$
ν_{xy}	Poisson's ratio	0.4	-
ν_{xz}	Poisson's ratio	0.4	-
ν_{yz}	Poisson's ratio	0.4	-
η	Structural damping	0.1	-

1 subscript ij implies that the voltage is applied or charge is collected in the i direction for a displacement or force in the j direction; here x and y are the in-plane directions of the PVDF membrane

2 along the thickness of the PVDF

Table 2.3 Elastic and electric properties of the PVDF membrane.

Parameters	*Name*	*Value*	*Unit*
E	Young's modulus	5.4×10^9	$N.m^{-2}$
ρ	Mass density	1780	$kg.m^{-3}$
η	Structural damping	0.05	-
ν	Poisson's ratio	0.18	-
h	Thickness	28×10^{-6}	m
e_{zx} [1]	Piezoelectric strain constant	0.03599	$C.m^{-2}$
e_{zy} [1]	Piezoelectric strain constant	0.13087	$C.m^{-2}$
ϵ_{zz} [2]	Permitivity	1×10^{-10}	$F.m^{-1}$

Table 2.4 Elastic properties of the bonding material

Parameters	*Name*	*Value*	*Unit*
E	Young's modulus	1×10^9	$N.m^{-2}$
ρ	Mass density	1300	$kg.m^{-3}$
η	Structural damping	0.1	-
ν	Poisson's ratio	0.4	-
h	Thickness	2×10^{-4}	m

CHAPTER 3

Active sound control with smart foams using piezoelectric sensoriactuator

Avant-propos

Authors :
A. Kundu : étudiant en maîtrise, Université de Sherbrooke, Faculté de génie, Département de génie mécanique.
A. Berry : professeur, Université de Sherbrooke, Faculté de génie, Département de génie mécanique.
Date of Submission : 08 April 2010
Journal : Journal of Intelligent Material Systems & Structures
Manuscript Number : JIM-10-045
Status : under review
Titre français : Contrôle actif de bruit avec les mousses actives à l'aide de 'sensoriactuator' piézoélectrique
Contribution of the document :
This paper presents the numerical simulation results and the experimental implementation of active sound control inside an impedance tube using piezoelectric sensoriactuators as the error sensor. The charge response of the piezoelectric actuator due to its mechanical strain has been isolated from the total charge response using an adaptive algorithm, and it has been used to implement a virtual error control strategy which is equally applicable for absorption and transmission control problems. Impressive results have been obtained with this self-sensing strategy for active control of propagating acoustic waves inside a waveguide. The proposed methodology of using piezoelectric sensoriactuators in active sound control domain is unprecedented and can offer compact and efficient solutions in practical aerospace configurations where an elaborate arrangement of far-field pressure sensors may not be always desirable. Hence the study concentrates on an important aspect of the application of smart foam technology to noise control applications and is a key part of the present masters project.
Résumé français :
Les mousses actives sont une solution de matériau léger et efficace pour le contrôle du bruit.

Elles combinent les avantages complémentaires de dissipation passive dans le matériau mousse avec l'autorité du composant piézoélectrique actif, sous un contrôle approprié. Cette étude vise à mettre en œuvre l'opération capteur/actionneur du composant actif piézoélectrique, avec l'objectif d'obtenir un signal alternatif d'erreur de la réponse de sa déformation mécanique. Cela peut éventuellement remplacer l'utilisation de capteurs d'erreurs microphoniques en champ lointain dans les applications de contrôle actif du bruit et donc, d'améliorer la compacité du système. Le sensoriactuator a été mis en œuvre en pratique avec la compensation analogique-numérique hybride de la "capacite feedthrough" de l'actionneur, à l'aide d'un algorithme adaptatif. La réponse de la charge mécanique, ainsi obtenue, a été minimisée en utilisant un algorithme fx-LMS et son effet sur l'indice d'affaiblissement a été étudié. En outre, il a été également utilisé dans l'absorption et les problèmes de contrôle de la transmission, en utilisant une stratégie de détection virtuelle, pour obtenir le contrôle de performance désiré en réduisant au minimum un signal d'erreur estimé virtuel. Les résultats expérimentaux ont été complétés par des résultats de simulation par éléments finis du système de contrôle du bruit, et ils fournissent une meilleure compréhension du problème physique de la réalisation de la mousse active 'sensoriactuator' et son applicabilité dans différents scénarios de contrôle de bruit.

3.1 Abstract

Smart foam offers a light weight, efficient noise control solution by combining the complementary advantages of passive dissipation in the foam material with the actuation authority of the active piezoelectric component, under appropriate control input. This study aims to implement the sensoriactuator operation of the active piezoelectric component to obtain an alternate error signal from its mechanical strain response. This can potentially replace the use of far-field microphone error sensors in active noise control applications and hence improve the compactness of the system. The piezoelectric sensoriactuator has been implemented with the hybrid analog-digital compensation of the quasi-stable feedthrough capacitance of the actuator using an adaptive algorithm. The mechanical charge response, thus obtained, has been minimized using an adaptive algorithm and its effect on the transmission loss has been studied. Additionally, it has also been utilized in absorption and transmission control problems, using a virtual sensing strategy, with the aim of obtaining the desired control performance by minimizing an estimated virtual error signal. The experimental results are supplemented with finite element

simulation of the coupled noise control system, and it provides a significant insight into the physical problem of the realization of the smart foam sensoriactuator.

3.2 Introduction:

A smart foam provides a hybrid passive-active approach for active noise control problems by integrating a distributed piezoelectric actuator into a passive sound absorbent material. While the passive material performs satisfactorily at high frequencies in terms of attenuation of the incident sound wave, the active actuator takes over at low frequencies, where the efficiency of the passive layer is limited by space and weight requirements. Previous studies with smart foam have shown good noise control effectiveness (over specific frequency bandwidths) in acoustic radiation control problems [Fuller *et al.*, 1996, 1994] and also in enhancing the broadband absorption coefficient for normally incident plane waves [Leroy *et al.*, 2009b; Leroy, 2008]. Recent study on the transmission control problem with smart foam reveals its capability in creating an acoustic isolation on the transmission side (downstream of the smart foam) under optimum control input [Kundu *et al.*, 2009; Kundu and Berry, 2010].

The previous works, concerning the absorption or transmission loss control of smart foams, derived the error with directional microphones sensors placed inside the waveguide to measure the sound waves reflected or transmitted by the smart foam. This can be impractical in a number of noise control situations, mainly due to the following reasons: introduction of sensors in acoustic domains, the requirement of minimal distance between the error microphone and the smart foam in order for the former to be sensitive only to propagative wave components and the severe causality constraint that has been observed in the study of active absorption [Leroy, 2008]. For such reasons, it is desirable to derive alternate error signals for active control to be integrated as much as possible to the sensing capability to the smart foam itself.

Hence, the present study looks to derive an alternate error signal from the mechanical strain response of the piezoelectric actuator of the smart foam, and thus use the active piezoelectric transducer simultaneously for actuation and sensing. A review of the different self-sensing techniques of piezoelectric devices can be found in the reference [Moheimani, 2003]. Two principal approaches concerning this can be identified in the literatures: one of them is to apply the same voltage across the piezoelectric transducer and an 'identical' capacitor (whose value is close to that of the physical transducer) and subtract the two electrical signals to resolve the mechanical response of the structure [Dosch *et al.*, 1992].

However, this suffers from the limitation of obtaining an accurate estimation of the electromechanical properties of the piezoelectric device, which generally exhibit a temporal variation with changing operating and environmental conditions and thus may destabilize the closed-loop performance of the sensoriactuator. This problem has been addressed in the alternate method of an adaptive sensoriactuator implementation based on a least mean square (LMS) algorithm [Clark *et al.*, 1996; Vipperman and Clark, 1996], which performs an online estimation of the '*feedthrough capacitance*' of the piezo-transducer using an adaptive gain imposed on the electrical circuit for compensation. Thus, the approach in effect allows a hybrid analog-digital electrical circuit to model the electrical response of the piezoelectric device, and extract the sensor signal using a compensator.

The piezoelectric sensory response has been utilized in the present study, as an alternative to microphone error sensors to control the transmission loss of the smart foams. A finite element simulation of the vibration response of the smart foam prototype demonstrates that minimizing the volume velocity (or displacement) of the piezo-actuator leads to minimising the transmitted sound wave within a limited frequency bandwidth. The volume displacement, for our smart foam design, turns out to be proportional to the electrical displacement (due to its mechanical deformation) of the piezo-sensoriactuator. The feedforward control that has been implemented with this error signal aims to achieve the desired attenuation of the transmitted sound wave by minimizing the vibration response of the piezoelectric membrane of the smart foam.

In addition to this, the piezoelectric self-sensing technique can also be utilized to formulate a virtual sensing algorithm, with which the desired attenuation of propagating sound waves can be achieved using the physical smart foam self-sensor placed remotely from the actual position of microphone error sensors. Previous studies concerned with virtual sensing techniques have shown its potential in improving the performance of local active noise control systems. The remote microphone technique [Roure and Albarrazin, 1999] requires a preliminary identification of the different transfer paths of the noise control system and modeling them as finite-impulse response (FIR) filters. Typically, two different FIR filters were identified apart from the plant identification (which is a part of the standard FX-LMS algorithm) to model the virtual error microphone reading from the measurements of the physical error sensors (remote microphones) viz. the FIR filter modeling the response of the virtual error sensor to the physical sensor under the action of primary source, and the impulse response of the virtual sensor to a secondary source perturbation. Thereafter the virtual sensing data is obtained from the physical sensor reading using a transform matrix and an adaptive algorithm is utilized to minimize the virtual error. This method usually

requires an accurate estimation of the FIR filters for efficient sound attenuation, and it has also been shown that the methodology lacks robustness in case of an erroneous estimation of the system transfer paths during identification phase. Another approach can be found in the works of Elliott *et al* [Elliott and David, 1992] which assumed the primary sound pressures at the physical and virtual error sensor positions to be identical (at least in the low frequencies) and for the secondary sound, the transfer functions for the physical and virtual locations are obtained in the preliminary identification stage and modeled as FIR or infinite-impulse response (IIR) filters. Peterson *et al* [Peterson *et al.*, 2006] proposed a method of estimating the virtual error signal at a moving virtual microphone location inside an acoustic duct and using a modified filtered reference least mean square (FX-LMS) algorithm to minimize the the virtual error. The Kalman filtering theory has also been used to implement the virtual sensing strategy to good effect [Peterson *et al.*, 2007]. Here, the optimal estimates of the error signals at the virtual locations are computed using the state-space model equations from the physical error sensor output data and the current estimate of the virtual error signal is fed into an FX-LMS algorithm to obtain real-time noise attenuation at the desired zones of quite removed from the physical error sensor. This method has been demonstrated to be effective in simple acoustic duct arrangements, and also has the potential to be extended to other practical three-dimensional sound fields in complex enclosures.

Thus the primary objective of the present study is to utilize the sensoriactuator behavior of the piezo-actuator embedded in the smart foam material and study its effectiveness as an error sensor for active transmission control problem. The virtual error sensor control algorithm has also been exploited for both transmission and absorption control, with a view to replace the use of any error microphone inside the acoustic waveguides, and observe the effectiveness of the self-sensing response in identifying the propagating wave magnitudes. This paper has been arranged as follows. Section 3.3 details the description of the noise control system and the smart foam prototype that has been used in our study along with the equations for evaluating the optimal control input and the acoustic energy indicators (absorption coefficient and transmission loss). A brief overview of the implementation of the piezoelectric sensoriactuator is given in section 3.4.1, and the finite element simulation results of the noise control system under the control of the sensoriactuator response is detailed in section 3.4.2. Experimental implementation of the minimization of the mehcanical charge response of the piezo-sensoriactuator using feedforward control is presented in section 3.4.3. The mathematical realization of the virtual control algorithm and its implementation in absorption and transmission control problems is described in detail in sections 3.5.1 and 3.5.2 respectively.

3.3 Description of the noise control system

3.3.1 Experimental Setup

The details of the smart foam and the physical noise control system used to implement the active absorption and transmission loss (TL) control are described in this section. The smart foam is located inside a plexiglass cavity which has impedance tubes attached on both of its sides. The frequency range of interest is restricted to well below the cut-off frequency (2200 Hz) of plane wave propagation of the impedance tubes.

The complete physical noise control set-up and the inter-microphone spacings on the incidence and transmission side waveguides are shown schematically in Figure 3.1. The primary source comprises of two speakers placed face to face of each other at one end of the tube and perpendicular to the tube axis. Electret microphones, placed along the length of the impedance tubes, are utilized in pairs to evaluate the propagating wave amplitudes and hence record the efficiency of control. The different inter-microphone spacings ensure an accurate estimate of the propagating wave amplitudes at all frequencies. The transmission side waveguide behind the plexiglass cavity ends in a rigid termination. The different

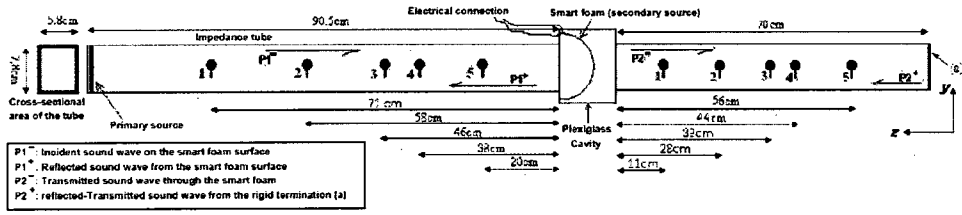

Figure 3.1 Physical Noise Control System with microphone positions along the length of the impedance tubes

propagating wave components have been indicated in Figure 3.1 which are evaluated with the help of microphone pairs using the classical two-microphone method [ASTM-E1050-98, 1998]. Also, a unidirectional electret microphone is placed inside the transmission side waveguide at a distance of 45 cm from its right end rigid termination. It faces the smart foam and is used to detect the transmitted sound wave. It is ideally assumed that there is no other acoustic transmission path between the incidence and transmission side waveguides other than through the smart foam. However, this assumption is not quite accurate for the actual physical noise control system assembly, as can be seen in the experimental results at low frequency.

For the absorption control experiments, the unidirectional microphone is placed approximately 20 cm from the free surface of the smart foam inside the absorption side impedance

tube, and facing the smart foam. It is utilized to detect the propagating wave which is reflected from the smart foam surface (indicated as $P1^+$ in Figure 3.1).

3.3.2 Smart Foam: Description

The smart foam used in our study is a composite noise control treatment consisting of a distributed polyvinylidene fluoride (PVDF) actuator, embedded within a layer of partially reticulated Melamine foam. It consists of half a cylinder of foam material with its curved rear surface covered with a PVDF film actuator. Since, melamine is highly porous, its surface is conditioned with a heat-reactivatable membrane and the PVDF is bonded onto it using a double-side tape. The bottom rectangular face of the smart foam is exposed to the normal plane acoustic waves. The thickness of the PVDF membrane is 28 microns,

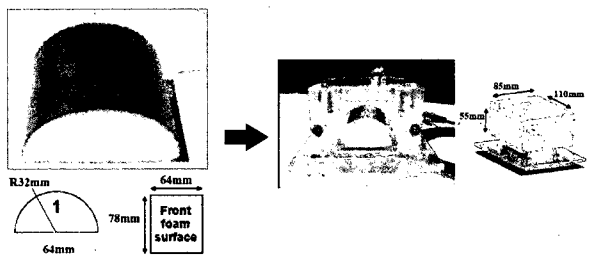

Figure 3.2 Smart foam prototype and the plexiglass cavity

and it possesses Cu-Ni surface electrodes. The elastic and electrical property values of the PVDF membrane used in the numerical simulations are listed in Table 3.1. The smart foam system is mounted inside the plexiglass cavity equipped with electric connections used for driving the PVDF actuator, as is shown in Figure 3.2. Plexiglass flanges are placed on the lateral sides of the foam so as to ensure proper support conditions and tightness with the rear cavity.

The curved shape of the PVDF membrane enables a strong coupling of the in-plane displacement components with the out-of-plane displacement. Since we assume an ideal condition of no acoustic leakage or flanking transmission paths between the incidence and transmission side waveguides, the transmitted sound pressure is solely a function of the vibro-acoustic response of the PVDF membrane, and the passive TL offered by the smart foams is quite high, especially at low frequencies. The absorption coefficient is also dependent on the vibration response of the PVDF membrane in addition to the passive dissipation in the foam material [Kundu and Berry, 2010].

3.3.3 Absorption Coefficient and Transmission Loss measurements

The complex propagating wave amplitudes have been derived using the Chung and Blaser method [Chung and Blaser, 1980], and the ASTM E1050 standard method [ASTM-E1050-98, 1998] with the several microphone pairs placed along the length of the tube and under the assumption of plane wave propagation. The 'offline' estimation of the optimal control input required to cancel a desired propagating pressure wave component is obtained utilizing the principle of superposition. Firstly, the system response under the action of the primary and secondary source (PVDF) inputs are evaluated separately. And then the optimal complex secondary source inputs, $\widetilde{\beta}^{+}$ or $\widetilde{\beta}^{-}$, required to cancel the reflected sound wave (propagating in the positive z-direction) or the transmitted sound waves (propagating in the negative z-direction) respectively, are calculated using the following expression -

$$\widetilde{\beta}^{\pm} = - \frac{\widetilde{H}p_{nm} - e^{\mp ikd}}{\widetilde{H}s_{nm} - e^{\mp ikd}} \tag{3.1}$$

where $\widetilde{H}p_{nm}$ and $\widetilde{H}s_{nm}$ are the transfer functions between microphone pairs under the action of the primary and secondary sources respectively and are expressed as $\widetilde{H}_{nm} = \frac{\widetilde{P}_n}{\widetilde{P}_m}$. The calculated $\widetilde{\beta}^{\pm}$ is a non-dimensional quantity which is normalized with the incident sound pressure amplitude of the primary source to obtain the desired control voltage input of the PVDF actuator per Pascal of the incident sound pressure. All these expressions are valid for the $e^{+i\omega t}$ time convention.

The acoustic energy indicators that have been monitored during the course of this optimization of control input are the absorption coefficient (α) and the Transmission Loss (TL) which are defined as in Equations 3.2 and 3.3:

$$\alpha = 1 - \left| \frac{\widetilde{P}_1^{+}}{\widetilde{P}_1^{-}} \right|^2 , \tag{3.2}$$

$$TL = 10 log_{10} \left| \frac{\widetilde{P}_1^{-}}{\widetilde{P}_2^{-}} \right|^2 . \tag{3.3}$$

where $\widetilde{P}_1^{-}$, $\widetilde{P}_1^{+}$ and $\widetilde{P}_2^{-}$ are the complex amplitudes of the propagating incident, reflected and transmitted pressure waves respectively (refer to Figure 3.1). These energy indicators are key parameters in defining the performance of the noise control system and determining the efficiency of control.

3.4 PVDF sensoriactuator

The principle of sensoriactuator that has been utilized in the present work for the active control of acoustic field, may present interesting alternatives to using microphone pressure sensor arrays. Previous studies with self-sensing piezoelectric sensoriactuators have shown that an accurate compensation of the 'feedthrough capacitance' of the piezo-actuator in-situ is the key towards isolating their sensory response, which is generally several orders of magnitude lower than the capacitor current. The following section gives a brief overview of the theory and the implementation of the PVDF sensoriactuator.

3.4.1 Piezoelectric Sensoriactuators

The sensoriactuator principle is based on the fact that electrical charge response of a piezo-actuator comprises in bulk portion of the capacitive electrical response (D_c) and the sensory response due to the mechanical deformation (D_m). The constitutive electromechanical equation for a typical linear piezoelectric material may be written as:

$$\{\sigma\} = [H]\{\epsilon\} + [\Theta]\{E\} \tag{3.4}$$

$$\{D\} = \underbrace{[\Theta]^T\{\epsilon\}}_{D_m} + \underbrace{[C_p]\{E\}}_{D_c} \tag{3.5}$$

where ϵ, σ, D and E are the strain, stress, electrical displacement (charge per unit area) and electrical field (volts per unit length) vectors respectively. In addition H, C_p and Θ are the stiffness, dielectric permittivity and piezoelectric coupling coefficient matrices of the piezoelectric material respectively. The total electrical displacement may thus be written as $D = D_c + D_m$. Vibration control or modal analysis typically requires the measure of the mechanical response of the sensoriactuator, and hence it is necessary to isolate the D_m from the total electrical displacement.

For the actuator design of the smart foam prototype considered in the present study, the in-plane displacement components of the PVDF membrane results in its predominant out-of-plane displacement. The electric displacement vector $[D]$ reduces to its third component only, along the z-direction (thickness direction) [Leroy *et al.*, 2009a]. Similar line of argument reduces the permittivity matrix $[C_p]$ into the coefficient c_{33} with the electric field E_z applied across the thickness of the PVDF membrane. Thus, the θ_{31} and θ_{32} elements of the piezoelectric strain constant matrix $[\Theta]$ are particularly important. The applied electric field along the thickness of the PVDF film may be expressed as $E_z = \Phi/h$, where Φ is the electric potential and h is the thickness of the film (28 microns). The scalar

electrical displacement due to the mechanical deformation (d_m) may be written in terms of the in-plane strains as:

$$d_m = \theta_{31}\epsilon_{xx} + \theta_{32}\epsilon_{yy} \tag{3.6}$$

where ϵ_{xx} and ϵ_{yy} are the in-plane strain in the PVDF film in the axial and circumferential direction, with θ_{31} and θ_{32} being the piezo strain constants along those directions respectively.

The capacitance of the sensoriactuator is expressed in fractions of farads and is generally proportional to its permittivity (approximately 30nF in the present case). The displacement current J is obtained as the time derivative of the electrical displacement. Also the scalar total electric charge response (Q) is the surface integral of the electrical displacement (under the assumption of no free charges) for infinite parallel plate capacitor, which is approximately similar to the case being studied presently. Thus the total piezoelectric charge may be written as :

$$Q = \int d_m dA + c_p \Phi \tag{3.7}$$

where A is the total surface area and c_p is the capacitance of the PVDF film respectively. Thus to compensate the capacitance charge response and isolate the mechanical response it is necessary to use a reference capacitor c_r (close to c_p), subjected to identical voltage inputs, such that the Equation 3.7 can be rewritten as

$$Q = \int d_m dA + (c_p - c_r)\Phi \tag{3.8}$$

Now, since the feedthrough capacitance of the piezo-actuators tend to exhibit temporal variations with changing environmental and operating conditions, a fixed value of the reference capacitor generally degrades the resolved mechanical response even if c_r is quite close to c_p. To account for this, the approach of adaptively altering the gain imposed on the compensation electrical circuit is adopted. This method of identification and online compensation of the feedthrough capacitance, which is presented in the works of Clark et al [Clark *et al.*, 1996; Vipperman and Clark, 1996], has been utilized in the present study to obtain the mechanical response of the PVDF membrane of the smart foam. Hence the action of the piezoelectric sensoriactuator, realized with this method, has been utilized to study their effectiveness in cancellation of the transmitted sound wave (explained in detail in section 3.4.3)

3.4.2 Finite element simulation

Finite element simulation of the complete noise control system is presented here to gain an in-depth physical understanding of the action of the smart foams in canceling the desired propagating sound waves. The simulations have been done with harmonic primary and secondary source disturbances introduced into the system over a frequency bandwidth of $25-1500$ Hz in steps of 25 Hz, and these frequency domain data are utilized to calculate the acoustic energy indicators and the optimal control input required to obtain the required control performance.

Description of the finite element model :

A 3-D finite element modeling of the complete noise control system shown in Figure 3.1 (including acoustic, elastic, piezoelectric and poroelastic domains) is described here. The finite element model for the poroelastic medium is based on an exact (u, p) formulation of the poroelastic domain [Atalla *et al.*, 2001; Debergue *et al.*, 1999]. The modeling utilizes quadratic poroelastic, elastic, fluid and piezoelectric elements to implement the weak integral formulation of these different media involved in the problem along with the associated coupling and boundary conditions [Leroy *et al.*, 2009a; Leroy, 2008].

The primary loudspeaker has been modeled with a fixed harmonic displacement imposed on all the nodes of the left waveguide termination on Figure 3.1, while the electrical excitation imposed on the PVDF membrane has been modeled with a fixed harmonic electric potential imposed on the piezoelectric domain. The boundary conditions imposed on the PVDF membrane are of particular importance to the radiation efficiency of the smart foams, since they significantly modify the relative structural modal contributions in its vibration response. The curved edges of the PVDF membrane have all their nodal translational degrees of freedom (d.o.f.) blocked while the straight edges have all (both their translational and rotational) d.o.f. fixed to zero. The acoustic domain is assumed to be inside a perfectly rigid structure (the impedance tube and the plexiglass cavity). There is no pressure continuity between the acoustic elements on the incident and transmission sides of the waveguide, thus the transmitted sound pressure is solely a function of the vibratory response of the PVDF membrane which forms an impervious membrane on the rear side of the foam surface. The model assumes no acoustical leakage or flanking paths between the incidence and transmission sides of the smart foam across the plexiglass cavity.

Simulation Results :

The charge response of the PVDF membrane due to its mechanical deformation can be obtained from the finite element simulations using the expressions for in-plane strain components given in Equation 3.6. To realize this, a schematic diagram of the circumferential and axial deformations is given in Figure 3.3, which shows the displacement components along the axial, circumferential and radial directions. The PVDF membrane, in the present

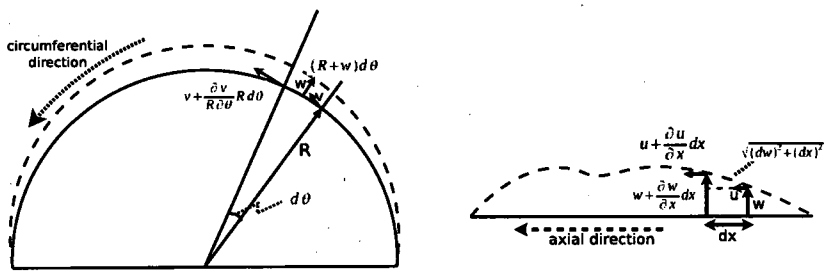

Figure 3.3 Strain in the PVDF membrane along the circumferential and axial directions

case, has negligible thickness compared to its circumferential and axial dimensions, and hence it can be appropriately assumed to behave like a thin membrane. It is assumed that only extensional strains are present, and any bending or shearing effects are neglected. To deduce the expression for circumferential strain ϵ_{yy}, we assume an average out of plane displacement w for each piezoelectric element aligned along this direction and proceed as follows:

$$\epsilon_{yy} = \frac{(R+w)d\theta - Rd\theta}{Rd\theta} + \frac{\partial v}{R\partial\theta}$$

$$hence, \qquad \epsilon_{yy} = \frac{w}{R} + \frac{\partial v}{R\partial\theta} \tag{3.9}$$

where R is the radius of the half-cylindrical PVDF membrane, v is the tangential displacement and $d\theta$ is the small angle subtended by a PVDF element at the center of the cylinder. The expression for the axial strain ϵ_{xx} can be obtained using the following steps:

$$\begin{aligned}\epsilon_{xx} &= \frac{\sqrt{(dw)^2+(dx)^2} - dx}{dx} + \frac{\partial u}{\partial x} \\ &= \left[1 + \frac{1}{2}\left(\frac{\partial w}{\partial x}\right)^2 + \cdots\right] - 1 + \frac{\partial u}{\partial x}\end{aligned}$$

and neglecting the higher order terms in the binomial expansion we get

$$\epsilon_{xx} = \frac{1}{2}\left(\frac{\partial w}{\partial x}\right)^2 + \frac{\partial u}{\partial x} \tag{3.10}$$

where u is the in-plane displacement along the axial direction (x-direction). It is to be noted that in Equations 3.9 and 3.10, the term w/R is many orders of magnitude higher than the other terms contributing to the expressions of in-plane strain. This is mainly due to the curved shape of the PVDF film which couples the in-plane displacement components to the predominant out-of-plane displacement component. Hence the electrical displacement d_m (given in Equation 3.6) can be effectively approximated to $d_m \approx \theta_{32} w/R$. Hence the total charge response Q_m of the PVDF membrane is given by

$$Q_m \approx \int \theta_{32} \frac{w}{R} dA \approx \frac{1}{R} \theta_{32} V_d \tag{3.11}$$

where θ_{32} is the piezo strain constant along the circumferential direction and $V_d = \int w dA$ is the radial volume displacement of the piezo-actuator. Thus, minimizing the volume displacement (or velocity) of the PVDF film can be expected to produce identical results to the minimization of the total mechanical charge response (or the total mechanical displacement current).

As a next step, the simulation results of the noise control system with the smart foam prototype is presented. Figure 3.4 shows the frequency domain response of the acoustic energy indicators, the absorption coefficient and the transmission loss, under passive operating conditions (no electrical voltage applied to the PVDF membrane). The transmission loss curves are plotted for the cases of a rigid termination and an anechoic termination implemented at the right end of the transmission side impedance tube (for details of the methodology of implementation of the anechoic termination, see reference [Kundu *et al.*, 2009]). The effect of the transmission side standing waves are clear at the frequencies where the 'rigid-termination' TL (in Figure 3.4(b)) decreases sharply.

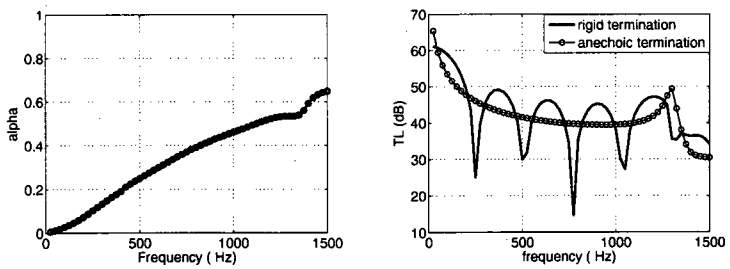

(a) (b)

Figure 3.4 Passive response of the noise control system under the action of primary source: (a) Absorption Coefficient (b) Transmission Loss

The control inputs for cancellation of the propagating transmitted sound wave is obtained using the expression involving the transfer functions between the microphones placed along the length of the waveguide (given in Equation 3.1). Following this, the optimal

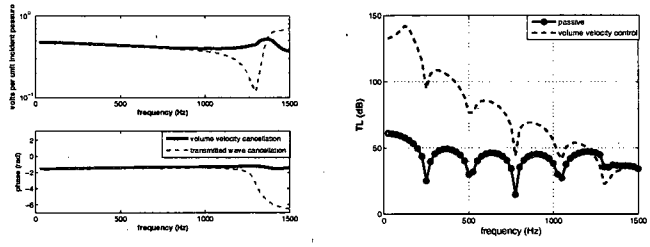

(a) (b)

Figure 3.5 Comparison of radial Volume Velocity cancellation of the PVDF membrane and transmitted sound wave cancellation: (a) optimum control input (b) Transmission Loss

control input required to cancel the net volume displacement (or velocity) of the PVDF sensoriactuator is calculated and modification of the transmission loss is observed under this optimum input applied to the PVDF film of the smart foam. Figure 3.5 shows a comparison of the optimum control inputs for the two cases. The magnitude of the control input has been normalized with the amplitude (in Pascal) of the incident pressure wave on the foam surface, and the phase response has been calculated with respect to the total fluid velocity on the foam surface. The curves show an identical trend until 1000 Hz. This can be used to justify the fact that transmission control with smart foams especially at low and mid-frequencies is accomplished by minimizing the vibration response of the PVDF membrane. At these frequencies the fundamental mode (1,1) of the PVDF shell is predominant and hence TL control effectively stalls its motion entirely. Beyond 1000 Hz however, when the relative modal amplitudes of the higher PVDF modes increases, the minimization is accomplished by the vibration restructuring of the PVDF membrane. The TL curve shown in Figure 3.5(b) indicates an improvement in passive TL value below 1000 Hz, under optimal control input for volume velocity minimization, which supports the view. It is to be noted that theoretically we get a complete cancellation of the propagating transmitted sound wave, under optimal control of the propagative transmitted sound wave, as given by Equation 3.1.

Delving further into the question of vibration restructuring of the PVDF membrane for TL optimization, it can be said that, the sound wave radiated on the transmission side waveguide is significantly influenced by the presence of the irregular geometry of the plexiglass cavity hosting the smart foam (the free field acoustic radiation can be expected to be quite

different). At high frequencies, the cancellation of the far-field propagating transmitted wave does not ensure a zero acoustic near-field behind the smart foam. Under optimal control with far-field microphones, the electrical input to the PVDF film produces those vibration mode shapes, which are responsible for far-field radiation, in equal amplitude and exact phase opposition to that induced due to the primary perturbation. However, the evanescent acoustic modes create a near field even when the far-field sound pressure has been minimized.

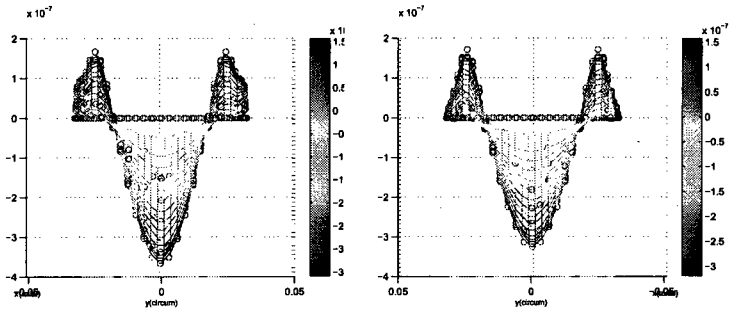

(a) (b)

Figure 3.6 PVDF deformation (projected view) for far-field pressure control at 1500 Hz: (a) passive (b) active

This can be verified from Figure 3.6 which shows the deformation shape of the PVDF film along the circumferential direction before and after control of the far-field acoustic pressure (transmitted sound wave) at 1500 Hz. It shows that the (3,1) mode of the PVDF film is predominant at this frequency and very little reduction of the displacement amplitude of the PVDF membrane is observed after control. Hence the cancellation of the far-field pressure is not concerned with the minimization of the net volume velocity at high frequencies, rather it deals with the vibration restructuring of the PVDF film so as to control its far-field radiation.

3.4.3 Experimental implementation of the PVDF sensoriactuator

The experimental studies of the volume displacement (or velocity) control of the PVDF membrane with a view to control the transmitted sound wave is presented in this section. As shown in section 3.4.2 and also proved in Equation 3.11, a measure of the charge response (or the total displacement current) of the PVDF film due to its mechanical current can be taken to be approximately proportional to its net volume displacement (or velocity). This can then be used as an error signal for the implementation of filtered reference least mean square (FX-LMS) control, instead of the conventional error microphone used to detecting the local acoustic pressure or the propagating sound wave.

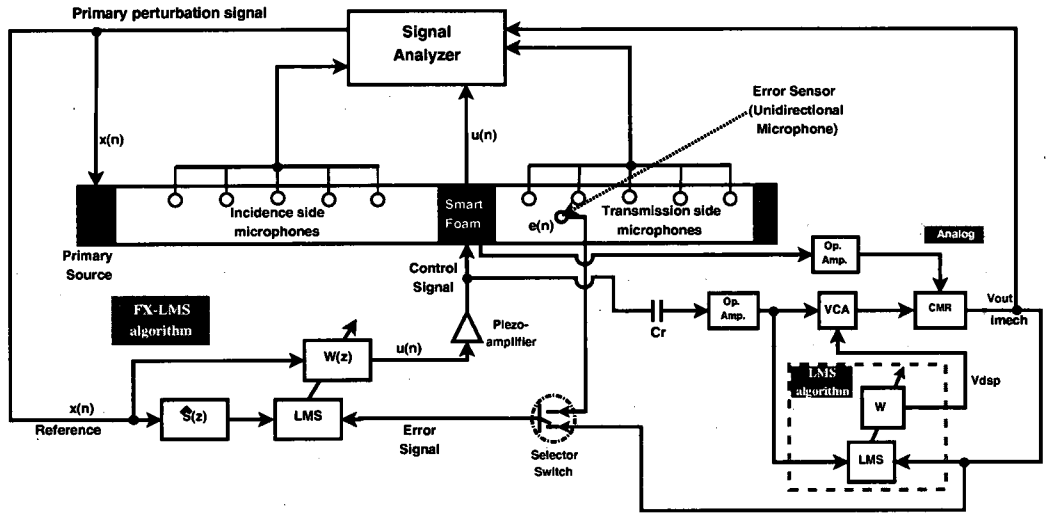

Figure 3.7 Feedforward active control of the transmitted sound wave, or the mechanical charge response of the PVDF sensoriactuator.

Figure 3.7 shows the block diagram of the feedforward active control strategy with the present configuration of the noise control system, and the error signal supplied either by the unidirectional error microphone placed inside the impedance tube or the mechanical charge response of the PVDF sensoriactuator. The 'FX-LMS' block shows the optimal control filter $W(z)$ and the identified plant transfer function $\widehat{S}(z)$ (either between the PVDF applied voltage and the unidirectional microphone voltage or between the PVDF applied voltage and the PVDF mechanical charge response). In order to resolve the mechanical response of the piezo-actuator from the electrical response, an adaptive compensation of the feedthrough electrical capacitance of the PVDF film has been implemented as is shown in Figure 3.7. It is seen that the compensation is performed by adaptively altering the gain imposed on the analog electrical circuit using a digital signal processing platform. A reference capacitor c_r has been used to produce an identical phase response with the main leg of the circuit (containing the actual piezo-actuator smart foam assembly) and VCA and CMR denote the blocks for 'voltage control amplifier' and 'common mode rejection' circuit respectively (see reference [Clark *et al.*, 1996] for details). An AD632 analog multiplier chip has been chosen to implement the functionalities of VCA and CMR. The adaptive compensation has been performed with a single coefficient FIR filter W, which is equivalent to the output voltage V_{DSP}. The voltage output from the CMR circuit can be written as:

$$V_{out}(s) = \underbrace{\frac{V_{DSP}(-sR_2c_rV_{pa}(s))}{10V}}_{reference\ leg} - \underbrace{sR_1c_pV_{pa}(s) - R_1i_{mech}(s)}_{primary\ leg} \tag{3.12}$$

where R_1 and R_2 are the gain resistors used with the Operation Amplifiers (shown as 'Op. Amp.' in Figure 3.7) in the primary leg and reference leg respectively, c_p is the capacitance of the PVDF membrane, c_r is the reference capacitor, V_{pa} is the voltage output from the piezo-amplifier that is supplied to the sensoriactuator and the reference capacitor, i_{mech} is the current response of the PVDF membrane due to its mechanical deformation, $10V$ is an internal gain in the AD632 multiplier chip and s is the Laplace variable. The objective of the adaptive compensation of the capacitor current response of the PVDF sensoriactuator is to minimize the portion of the CMR output that is coherent with the voltage response of the reference capacitor c_r, and hence isolate the current response due to the mechanical strain of the PVDF film. Thus, under perfect compensation of the capacitor charge response, when the expression for V_{out} is expected to be proportional to i_{mech}, the d.c. voltage input from the DSP to the adaptive circuit will be given as :

$$V_{DSP} \equiv \frac{(10V)R_1 c_p}{R_2 c_r} \tag{3.13}$$

This equation can also be utilized to dynamically determine the capacitance c_p of the piezo-actuator in-situ, which can generally point out to the discrepancy of the value of the capacitance measured with a standard multimeter.

Now, the results obtained with a feedforward FX-LMS minimization of the mechanical current response of the PVDF sensoriactuator is presented here and its effect on the TL of the smart foam is discussed. Figure 3.8 and 3.9 shows the comparison of the numerical mechanical current response of the PVDF film with the finite element results and the efficiency of this control in terms of PVDF vibration reduction. Figure 3.8(a) shows

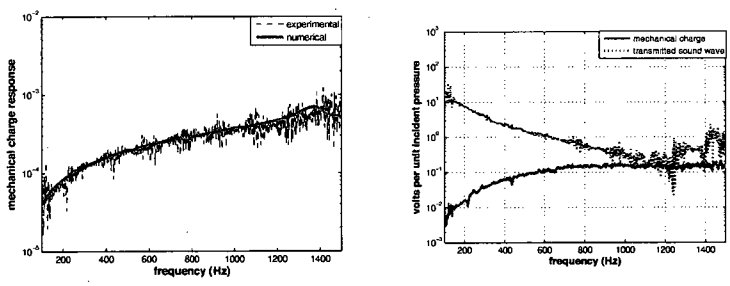

(a) (b)

Figure 3.8 (a) Comparison of the numerical and experimental mechanical current response of the PVDF film under primary perturbation (b) control input for minimization of the PVDF mechanical current and its comparison with optimal TL control input

that there is a fair agreement between the current response of the PVDF membrane for

the experimental and numerical results. The numerical charge response is approximately proportional to the volume velocity of the PVDF film (as shown in Equation 3.11) and has been scaled with a constant to bring it to the same order of magnitude as the experimental results. Figure 3.8(b) shows the control input required for the minimization of the mechanical current of the PVDF, and it is found to be quite less than the optimal control voltage for cancellation of the transmitted sound wave. This optimal control voltage has been calculated using the double microphone method following Equation 3.1.

The mechanical charge response of the PVDF sensor, however, is found to have been reduced substantially under the feedforward control as is shown in Figure 3.9(a). This also leads to a reduction in the velocity of the center of PVDF surface, which has been monitored with a single-point laser Doppler vibrometer (Figure 3.9(b)). The reduction of

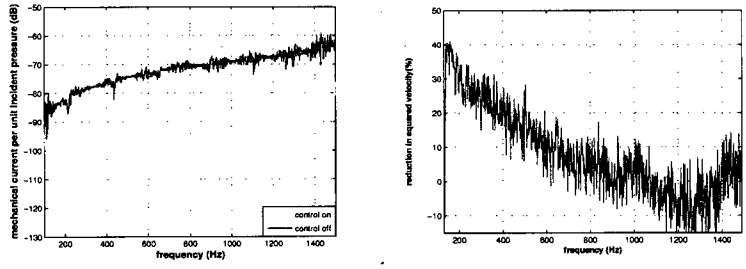

(a) (b)

Figure 3.9 Control of the PVDF mechanical current response : (a) Mechanical current response before and after control (b) percentage reduction in the squared velocity of the center of the PVDF film after control

the PVDF vibration response under minimization of the sensory charge response of the PVDF membrane is confirmed from this result, at least up to 800 Hz, beyond which the PVDF membrane response can be expected to be more complicated due the increase in contribution of the higher structural mode shapes. The comparatively lower level of vibration reduction of the PVDF membrane under active control of the mechanical current can be attributed to the effect of any residual sensory signals due to the modeling uncertainties, non-linear effects or inappropriate characterization of the piezoelectric and/or elastic bonding layer of the smart foam.

It has also been observed that the reduction of this mechanical current response of the PVDF membrane did not translate into any significant improvement in the TL of the smart foams. As an explanation of this phenomenon, it can be said that the auxiliary flanking acoustic paths from the incidence to the transmission sides of the smart foam (mainly through the vibroacoustic coupling of the structures involved like the waveguides

and the plexiglass cavity, and also acoustic leakage) results in decreasing the value of the passive transmission loss especially at low and mid-frequencies. This results in the PVDF sensor being unable to account for a large part of the transmitted sound pressure, and hence the minimization of the mechanical charge response has little or no effect on the transmitted pressure at the low and mid frequencies. This explanation can also be supported from the fact that the control voltage for the minimization of the mechanical current is significantly lower (especially at low and mid frequencies) than the optimal control voltage input required for cancellation of the transmitted sound wave. At high frequencies however, the mechanical current minimization is not expected to lead to good TL improvement as has been observed in the numerical simulation results in Figure 3.5(b), due to the increase in the modal amplitudes of the higher vibration mode shapes of the PVDF membrane.

Thus, it can be concluded that, the mechanism of control of the transmitted sound wave at low and mid frequencies is markedly different in case of the experimental studies compared to the simulation results, which assumes no auxiliary flanking paths between the incidence and transmitted sides of the smart foam, and hence the transmitted sound wave to be solely a function of the vibration response of the PVDF membrane. However, in case of the actual test setup, the flanking transmission paths are found to play a significant role especially at these frequencies when the vibroacoustic coupling of the waveguide and the plexiglass cavity is significant. Hence, the smart foam system, at these frequencies, basically acts as a secondary acoustic source, which operates on a feedforward control loop to minimize the flanking acoustic transmissions, and hence the PVDF vibration response is not well-correlated to the error microphone reading. Thus, practically no significant improvement in TL values has be obtained with this approach due to the gross inaccuracy of the experimental test setup. However, it can be asserted that under ideal conditions of acoustic transmission through smart foams, as has been assumed in the FEM simulations, minimization of the vibration response of the piezo-actuator may actually lead to TL improvement in the low and mid frequency ranges.

3.5 Virtual Sensing for active noise control

Local active noise control systems aim to produce zones of quiet at particular locations within a sound field. However, the resulting zones of quiet may be centered at the error sensors and are often too small to extend from the error sensors to the observer's ears. Virtual sensing methods are potential alternatives to circumvent this problem. Also, virtual sensing may be effective in improving the compactness of the system, which is a

necessity in aerospace applications, where an elaborate design of physical sensors at actual noise control locations can be substituted by virtual sensing algorithm. Using this it is possible to compute optimal estimates of the error signals at the virtual locations, which are remote from the actual physical locations of error sensors.

This approach has been shown to perform well in case of an active duct noise cancellation problem using feedforward control algorithm [Roure and Albarrazin, 1999; Peterson *et al.*, 2006]. In this paper we look to utilize the method of virtual sensing for minimizing the desired propagating acoustic waves inside the impedance tubes, instead of using the physical unidirectional microphone error sensor. The sensory response of the PVDF actuator of the smart foam will be utilized to model a virtual error signal, which when minimized will lead to the desired control effect at the removed locations from the PVDF sensor.

3.5.1 Virtual Sensing

In the present study, the physical error sensor which is used by the control system to construct the virtual error signal is appropriately removed from the location of actual error sensor (which would be the unidirectional electret microphone), and the minimization of desired propagating sound waves is accomplished by performing a preliminary FIR identification of some transfer paths of the noise control setup. The virtual error sensing strategy has been utilized both for the purpose of enhancing the acoustic absorption coefficient and TL of the smart foam.

To achieve this, typically two different FIR filters were identified apart from the secondary path model (which is a part of the standard fx-LMS algorithm) to model the virtual error signal, viz. the FIR filter modeling transfer path from the PVDF sensoriactuator to the unidirectional microphone sensor under primary perturbation, and the control filters required for the actual absorption or transmission loss control problem with error microphones. The method followed here can be considered similar in terms of computational complexity to that detailed in reference [Roure and Albarrazin, 1999], which makes use of identification of the transfer paths via FIR filters and combining them into the filtered reference algorithm to obtain an estimate of the virtual error signal.

Figure 3.10 shows the block diagram of the active noise control system having the smart foam inside the impedance tube, along with the PVDF sensoriactuator and the unidirectional microphone sensor, which is either on the incident side of the smart foam for reflected wave cancellation or on the transmission side for transmitted wave cancellation. Here $x(n)$ is the reference signal (the primary loudspeaker input), and $I_p(n)$ and $I_s(n)$ are

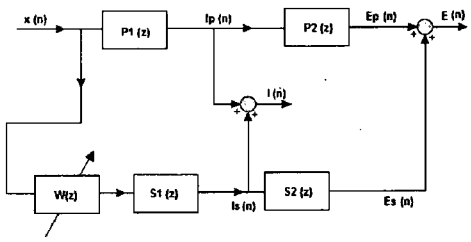

Figure 3.10 Block diagram of the absorption control problem

the mechanical charge response of the PVDF membrane due to the primary and secondary source perturbations respectively. Thus $P_1(z)$ and $S_1(z)$ are the transfer functions between the primary and secondary source inputs, and the PVDF mechanical current. The total mechanical current is thus obtained as $I(n) = I_p(n) + I_s(n)$. Under active control, the secondary source is driven by the optimal control filter $W(z)$ whose coefficients are updated in real time using the stochastic gradient estimation algorithm. Now the error microphone reading can be obtained as the sum of the acoustic pressures readings due to the primary and control source inputs, $E(n) = E_p(n) + E_s(n)$, where the error microphone reading $E_p(n)$ due to the primary source input can be expressed with a primary plant model $P_2(z)$ between the mechanical current and the error microphone under the action of the primary source, and $E_s(n)$ due to the secondary (control) source input can be expressed with the secondary plant model $S_2(z)$ between the mechanical current and the error microphone under the action of the secondary source.

The primary and secondary plant models $P_2(z)$ and $S_2(z)$ are very different from each other and hence a simple FIR model of the error microphone response (virtual) from the mechanical current data (physical sensor) will not give an appropriate virtual sensor measurement. Moreover, a mere minimization of the mechanical current can not be expected to yield any satisfactory control result. Thus, it is necessary to redefine and model an error signal using the physical sensor output (mechanical charge response of the PVDF membrane) and the reference signal (primary source input), such that minimization of this virtual error signal will ensure cancellation of the desired propagating sound wave.

To achieve this, the block diagram of the problem is presented once again in a modified form in Figure 3.11(a) (the error microphone signal has been omitted in this figure). The figure shows a way of constructing the virtual error signal by combining the reference signal and the PVDF sensory response, using two digital filters $V_1(z)$ and $V_2(z)$, such that we have a virtual error signal $\widehat{E}(n)$. Now, the choice of $V_1(z)$ and $V_2(z)$ needs to be so, that minimization of this error signal would also lead to the minimization of the error

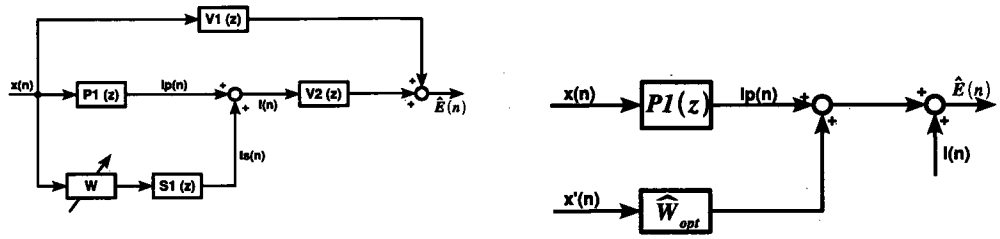

(a) (b)

Figure 3.11 (a) Modified block diagram (b) Virtual error signal block diagram

microphone reading. We can write the equation for the virtual error $\widehat{E}(z)$ as :

$$\widehat{E} = V_1 X + V_2 I$$
$$\text{or,} \qquad \widehat{E} = V_1 X + V_2(P_1 X + W S_1 X). \tag{3.14}$$

where W is the adaptive control filter that minimizes $\widehat{E}^2$. We choose the filters V_1 and V_2 in such a way that W has to converge to the previously identified control filter $\widehat{W}_{opt}$ of the absorption or TL control problem (with the conventional error microphone), for this virtual error control problem to be stable. A look at Equation 3.14 suggests that if we take $V_1 = (P_1 + \widehat{W}_{opt} S_1)$ and choose V_2 to be -1, then :

$$\widehat{E} = (P_1 + \widehat{W}_{opt} S_1)X \; - \; (P_1 + W S_1)X$$
$$\text{or,} \qquad \widehat{E} = (\widehat{W}_{opt} - W) S_1 X. \tag{3.15}$$

From Equation 3.15 it can be said that for the virtual error to be zero, it is necessary for W to converge to $\widehat{W}_{opt}$. Hence, once convergence is reached this would lead to a simultaneous minimization of the virtual error signal (modeled in Equation 3.14) and the signal at the unidirectional microphone, E.

Thus the estimation of V_1 requires the knowledge of P_1, $\widehat{W}_{opt}$ and S_1. Here, P_1 and $\widehat{W}_{opt}$ have to be estimated in a preliminary identification stage before taking up the feedforward virtual error control problem. P_1 is determined with an LMS identification of the primary path as an FIR filter. $\widehat{W}_{opt}$ is obtained from the actual Fx-LMS determination of the control filter coefficients for the absorption/TL control problem using the unidirectional microphone as the physical error sensor. The non-causally constrained control filter $\widehat{W}_{opt}$ can also be derived from the secondary plant and the power spectral densities of the reference and the perturbations. This would not necessitate to carry out the preliminary physical active control experiment with the unidirectional error microphone. The

frequency domain expression of this optimal casually unconstrained filter is given as:

$$\widehat{W}_{opt}(e^{j\omega T}) = -\frac{S_{xd}(e^{j\omega T})}{S_1(e^{j\omega T})S_{xx}(e^{j\omega T})} \tag{3.16}$$

where S_{xd} is the cross spectral density between the reference signal and the error microphone response, and S_{xx} is the power spectral density of the reference signal input. S_1, however, is the secondary plant transfer function and its estimation is a part of the feedforward control problem. S_1 is identified as an FIR filter using the LMS algorithm and is then used to generate the filtered reference signal. The filtered reference $x_n^{'}$ is easily obtained using the plant identification FIR filter and the reference signal as per the following equation:

$$x^{'}(n) = [s_0 \ ... \ s_{I-1}] \times [x(n) \ ... \ x(n-I+1)]^T \tag{3.17}$$

where s_j's are the I coefficients of the identified secondary plant and $x(n)$ is the reference signal at the discrete time step n. The block diagram for the method of obtaining the virtual error signal is given in Figure 3.11(b). The virtual error signal is thus a combination of the mechanical current and the primary input reference, and hence the method is strictly valid for the feedforward problem.

3.5.2 Experimental implementation

The virtual error control methodology and equations described above have been applied to the cases of absorption and TL control problems, by utilizing the sensory response of the PVDF sensoriactuator. The experiments have been designed with the objective of demonstrating the principle of smart foam sensoriactuators to be valid for active noise control problems. Control has been performed with a broadband disturbance over the frequency range of $100-1500$ Hz and the acoustic energy indicators (absorption coefficient and TL) monitored with the microphones placed along the length of the impedance tubes on the absorption and transmission sides of the smart foam. Both P_1 and $\widehat{W}_{opt}$ have been identified as FIR filters having 250 coefficients each.

Absorption Control :

The primary path FIR filter P_1 and the optimal control filter $\widehat{W}_{opt}$ for the absorption control problem have been identified prior to the actual virtual control problem with the unidirectional microphone as the physical error sensor. Using these the virtual error signal has been modeled and implemented in the real-time active control problem. During the

actual experimental minimization of the virtual error signal, the unidirectional microphone has been left in its place to monitor the effectiveness of control.

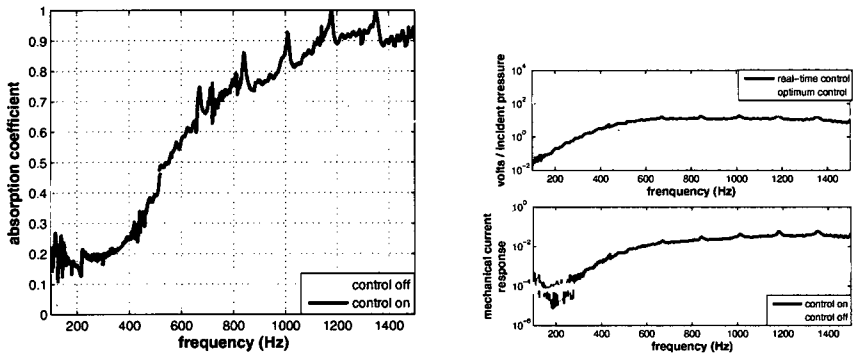

(a) (b)

Figure 3.12 Virtual error minimization for absorption problem (a) Absorption coefficient (b) Control input (top) and mechanical charge response (bottom) per unit pascal of the incident acoustic pressure amplitude

Figure 3.12 shows the results for the absorption control problem with the minimization of virtual error signal. The unidirectional microphone which has been utilized at the preliminary identification stage of the control problem has been placed approximately 20 cm from the free surface of the smart foam inside the incidence side impedance tube. It can be seen in Figure 3.12(a) that there is a large improvement of the absorption coefficient under control in the mid and high frequencies. The unsatisfactory control performance below 500 Hz can be attributed to the poor signal to noise ratio at the PVDF sensoriactuator. At low frequencies, which is way below the fundamental structural mode for the smart foam system, the PVDF response is very small and this deteriorates the efficiency of control.

Similar effect of the poor signal to noise ratio at the PVDF sensoriactuator can be observed in Figure 3.12(b), which shows the control input and the mechanical charge response of the PVDF film before and after control. The comparison of the optimum value of the control input (calculated with the impedance tube microphone pairs according to Equation 3.1) with the real-time control effort required to cancel the reflected sound wave shows that at low frequencies the actual control effort is significantly lower than the optimum value, which supports the lack of improvement in the value of absorption coefficient at low frequencies. The charge response due to the mechanical deformation of the PVDF film shows that the mechanical charge response increases significantly under control, to enable enhanced acoustic absorption by the smart foam.

Transmission Loss Control :

The transmission control problem similarly makes use of the previously identified FIR filters (the primary path FIR filter P_1 and the optimal control filter $\widehat{W}_{opt}$ for the transmission control problem) to model the virtual error signal, and then uses the classical filtered reference steepest descent algorithm to minimize this error signal. During the identification of these FIR filters, the physical unidirectional microphone has been placed behind the smart foam inside the transmission side waveguide facing the smart foam, and at a distance of 45 cm from the right end rigid termination of the tube.

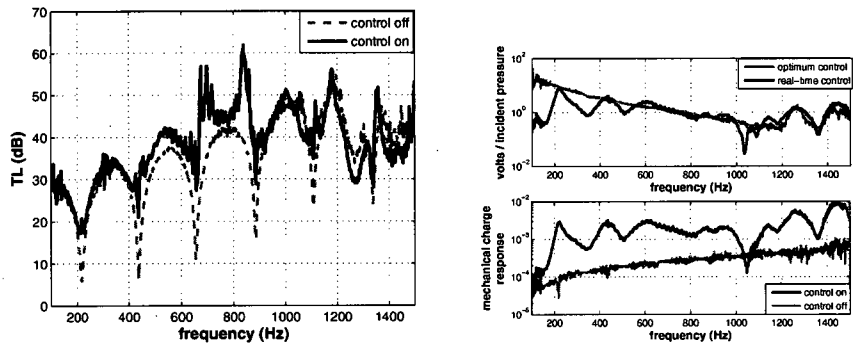

(a) (b)

Figure 3.13 Virtual error control for TL problem (a) Transmission loss (b) Control input (top) and mechanical charge response (bottom) per unit pascal of the incident pressure amplitude

It can be seen in Figure 3.13(a) that there is a fairly large improvement of the TL of the smart foam under control in the mid frequencies. Especially, at the standing wave frequencies of the acoustic wave on the transmission side impedance tube (where there the TL dips down to quite low values) there is a very good improvement in TL value, which can be attributed to the enhanced PVDF response at these frequencies. The unsatisfactory control performance at low frequency can again be attributed to the poor signal to noise ratio at the PVDF sensoriactuator, due to lower levels of mechanical strain induced in the PVDF film by the acoustic field.

The poor signal to noise ratio at the PVDF sensoriactuator can be observed similarly in Figure 3.13(b), which shows the control input required for the real-time control of the virtual error signal for the TL control problem and the mechanical charge response before and after control. The comparison of the optimum value of the control input (calculated using Equation 3.1) with the real-time control effort required to cancel the transmitted sound wave shows that below 400 Hz, the actual control effort is lower than

the optimum value. This indicates, similar to the active absorption problem, that the weak mechanical response of the PVDF membrane at low frequencies limits the effectiveness of control considerably. The control is found to be most effective in the mid-frequencies ($500-900$ Hz), while beyond 1200 Hz, the control results does not show any improvement in the passive TL value. This can be attributed to the fact that the increase in the value of passive TL at these frequencies (due to an increased passive absorption in the foam material) leads to a small transmitted wave amplitude and hence does not lead to appreciable TL improvement. However, this is open to further investigation.

The charge response due to the mechanical deformation of the PVDF film, in Figure 3.13(b) (bottom) shows that the mechanical charge response increases significantly under control, which helps to provide enhanced TL values by the smart foam. At low and mid frequencies, the bulk portion of the acoustic transmission takes place via the auxiliary flanking paths (due to the strong vibroacoustic coupling of the waveguide walls with the fluid domain) and the contribution due to the acoustic radiation of the PVDF membrane is quite small. Thus, it requires the smart foam to produce a secondary acoustic field that will cancel the primary perturbation, and hence an increase in the mechanical response of the PVDF membrane. Thus, the mechanism of control is contrary to stalling the motion of the PVDF membrane, as would have been expected in the case of acoustic transmission through the smart foam only and absence of all acoustic flanking paths.

3.6 Conclusion

It has to be mentioned out that the very encouraging results obtained with the PVDF sensoriactuator principle for these active noise control problems points to the fact that there is room for further improvement of smart foam design and performance of the active control error sensing strategy with the piezoelectric self-sensing strategy. These may help to alleviate the limited performance of active control strategy at low frequencies for the absorption problem, and improve the performance of the TL control problem at high frequencies.

The following important conclusions can be drawn from the investigation of the PVDF sensoriactuator of the smart foams in active noise control scenarios:

- The study shows that the sensoriactuator response is effective for cancellation of the propagating sound waves while operating on the virtual control algorithm.
- The virtual control technique used in the present study can be investigated further for its sensitivity and robustness in face of changing ambient and operating conditions.

- Low frequency operation of the PVDF sensoriactuator is limited by the small deformation of the PVDF membrane, which can surely be investigated further while optimizing the design of the smart foams.
- A direct minimization of the mechanical charge response for TL control problem however, is unable to produce satisfactory results, which may be largely attributed to the auxiliary flanking acoustic transmission paths in the physical noise control setup.

Future studies in this direction will be focused at addressing these problems, and further investigation into the possibility of deriving alternate error signals for active noise control from the vibration response of the smart foam components.

Acknowledgments

The authors would like to acknowledge the support of the Natural Sciences and Engineering Research Council of Canada, Bombardier Aerospace, Pratt & Whitney Canada and Bell Helicopter Textron Canada.

Table 3.1 Elastic and electric properties of the PVDF membrane.

Parameters	*Name*	*Value*	*Unit*
E	Young's modulus	5.4×10^{9}	$N.m^{-2}$
ρ	Mass density	1780	$kg.m^{-3}$
η	Structural damping	0.05	-
ν	Poisson's ratio	0.18	-
h	Thickness	28×10^{-6}	m
θ_{31}	Piezoelectric strain constant	0.03599	$C.m^{-2}$
θ_{32}	Piezoelectric strain constant	0.13087	$C.m^{-2}$
c_{33}	Permitivity	1×10^{-10}	$F.m^{-1}$

CHAPTER 4

GENERAL CONCLUSIONS

4.1 Summary of Principal results

The finite element study of the complete coupled noise control system points to the following facts:

- The Finite Element Model of the coupled noise control system developed at GAUS, Université de Sherbrooke predicts the sound absorption and transmission through the smart foams with sufficient precision, and it conforms to the experimental results.
- The absorption and transmission control problems are complementary to each other, in terms of the action of the piezo-actuator for canceling the respective propagating sound waves.
- For comparable volume of the smart foams (as is the case for the 3 designs of smart foam considered in our numerical simulations), the actuator design and its acoustic radiation efficiency has a significant influence on the acoustic energy indicators of the smart foam.
- Optimization of the TL of the smart foams is based on stalling the motion of the PVDF membrane below the fundamental mode of vibration of the smart foams, while at higher frequencies the vibration restructuring of the PVDF film ensures cancellation of the far-field radiating modes.
- The first design of the smart foam offers the highest passive TL, and hence requires the least control voltage per pascal of the incident sound pressure amplitude for complete cancellation of the transmitted sound wave.
- The absorption and transmission loss problems are appreciably decoupled for the first design of the smart foam, hence, TL control does not modify the absorption coefficient appreciably. This however, is not true for the second and third designs.
- The cancellation of the transmitted sound wave at low and mid-frequencies leads to minimization of the spatially averaged radial volume velocity of the PVDF membrane (under the idealized assumption of the absence of any auxiliary flanking acoustic transmission paths). This inspires the use of the radial volume velocity response of the PVDF membrane as an alternate error signal for active control instead of far-field unidirectional error microphones.

- The volume velocity of the PVDF film of the first smart foam prototype is almost equal to the charge response of the PVDF membrane due to its mechanical deformation. Thus, the sensory response of the active PVDF film can be directly used as the cost function to optimize the TL of the smart foam.

The experimental studies of the noise control system under primary perturbation and feedforward control help us to draw the following conclusions:

- The overestimation of the TL of the passive system in numerical simulations is attributed to the auxiliary flanking transmission paths, especially due to a strong vibroacoustic coupling of the waveguide walls with the fluid domain at low and mid frequencies.
- Good improvement in TL has been obtained under single frequency and broadband primary perturbation with SISO feedforward control.
- The performance of the active noise control system for broadband primary perturbation deteriorates beyond 800 Hz which is due to the poor signal to noise ratio at the error microphone.
- The sensory response of the PVDF film per unit incident pressure amplitude matches the same predicted by the numerical simulation, which indicates an appropriate realization of the sensoriactuator principle.
- Since the mechanical deformation of the PVDF membrane at low frequencies is very small (also indicated by the numerical simulation results), it leads to a poor signal to noise ratio in the PVDF sensory response at these frequencies.
- The poor control results at low frequencies for the absorption and transmission control problems operating on the virtual error sensing algorithm, can be explained in light of this poor PVDF sensory signal.
- The good control results obtained with the PVDF sensoriactuator (under virtual error sensing algorithm) demonstrates that the mechanical charge response of the PVDF membrane is well correlated to the far-field microphone response under primary and secondary source perturbations.
- The apparently unsuccessful TL control results at low and mid frequencies for the direct minimization of the mechanical charge response of the PVDF film can be attributed to the very low deformation of the PVDF membrane at these frequencies and also to the high acoustic transmission through the flanking paths.
- The preliminary studies with the PVDF sensoriactuator show its potential in using it as an integral part of the active control system, and can be used instead of conventional far-field microphones.

The above conclusions indicate that a thorough understanding of the mechanism of cancellation of propagating sound waves inside impedance tubes has been obtained from the numerical simulation results. The present study of sound transmission loss is one of its first kind of studies that has been undertaken in the domain of active acoustic isolation with smart foams. The complete experimental demonstration of the feedforward control of TL with smart foams has been presented in this work, which gives the control voltage input normalized with the amplitude of the incident sound pressure amplitude. This allows a relative comparison of the different designs of the smart foams in terms of the TL effectiveness under active control.

The implementation of the smart foam sensoriactuator for the control of far-field acoustic waves is a major originality of the present work. Deriving the error signal from the mechanical response of the smart foam has been attempted without success in previous studies, and thus the present work is an important step forward along this direction, which may encourage the investigation of alternate error signals for active control for use instead of far-field microphone pressure sensors. The virtual control algorithm proposed in the present study looks to combine the reference and the PVDF sensory response to deduce a virtual error signal. Though similar approaches have been tried previously in other control scenarios (e.g. the remote microphone technique), it has not been utilized in conjuncture with the PVDF sensoriacutator technology.

4.2 Future Work

The future work along this direction may focus on a number of interesting propositions. The study of acoustic absorption and isolation can be extended to the case of diffuse field primary perturbation, and free field radiation. The use of multiple smart foam prototypes operating on a centralized MIMO control algorithm and their effectiveness in controlling the acoustic modes with an array of microphones will be a key towards their applicability in practical industrial acoustic liners.

The use of the sensoriactuators in the control of acoustic far-field will be an important domain of future studies. The investigation of the minimization of the vibration response of the active piezo-transducer and its effect on the acoustic far-field will be a key to the successful implementation of the piezo-selfsensing technology in active noise control problems. Also, the use of virtual sensing algorithms presented in the present study, and other similar approaches may be quite important in the implementation of the active

acoustic liners, and a study of their sensitivity and robustness in face of changing ambient and operating conditions will be very useful.

LIST OF REFERENCES

ASTM-E1050-98 (1998) Standard test method for impedance and absorption of acoustical materials using a tube, two microphones, and a digital frequency analysis system. American Society for Testing Materials.

Atalla, N., Hamdi, M. A. and Panneton, R. (2001) Enhanced weak integral formulation for the mixed (u,p) poroelastic equations. *Journal of the Acoustical Society of America*, volume 109, no. 6, pp. 3065–3068.

Bailo, K., Brei, D. and Grosh, K. (2003) Investigation of curved polymeric piezoelectric active diaphragms. *Journal of Vibration and Acoustics*, volume 125, pp. 145–154.

Chin, C., Lee, J. and Mathur, G. (2002) Analytical modeling of active/passive smart foam noise control treatment in aerospace vehicles. In *8 th AIAA/CEAS Aeroacoustics Conference and Exhibit.*

Chung, J. Y. and Blaser, D. A. (1980) Transfer function method of measuring in-duct acoustic properties. I. Theory. *Journal of the Acoustical Society of America*, volume 68, pp. 907–913.

Clark, R. L., Vipperman, J. S. and Cole, D. G. (1996) Adaptive piezoelectric sensoriactuator. *U.S. Patent 5578761.* http://www.freepatentsonline.com/5578761.html.

Cobo, P., Fernandez, A. and Doutres, O. (December 2003) Low-frequency absorption using a two-layer system with active control of input impedance. *Journal of the Acoustical Society of America*, volume 114, no. 6 I, pp. 3211–3216.

Cobo, P., Pfretzschner, J., Cuesta, M. and Anthony, D. K. (October 2004) Hybrid passive-active absorption using microperforated panels. *Journal of the Acoustical Society of America*, volume 116, no. 4 I, pp. 2118–2125.

D'Angelo, J. (2004) Attenuation of turbulent boundary layer induced interior noise using integrated smart foam elements.

Debergue, P., Panneton, R. and Atalla, N. (1999) Boundary conditions for the weak formulation of the mixed (u,p) poroelasticity problem. *Journal of the Acoustical Society of America*, volume 106, no. 5, pp. 2383–2390.

Dosch, J. J., Inman, D. J. and Garcia, E. (1992) A self-sensing piezoelectric actuator for collocated control. *Journal of Intelligent Material Systems and Structures*, volume 3, no. 1, pp. 166–185.

Elliott, S. and David, A. (1992) Virtual microphone arrangement for local active sound control. In *Proceedings of 1st International conference on motion and vibration control.* pp. 1027–1031.

Elliott, S. J. (2001) *Signal Processing for Active Control.* Academic Press.

Fuller, C. R., Bronzel, M. J., Gentry, C. A. and Whittington, D. E. (May 1-4 1994) Control of sound radiation/reflection with adaptive foams. In *Proceedings of the 1994 National Conference on Noise Control Engineering*. Virginia Polytechnic Inst and State Univ, Blacksburg, VA, USA, pp. 429–436.

Fuller, C. R., Guigou, C. and Gentry, C. A. (Feb 27-29 1996) Foam-pvdf smart skin for active control of sound. In *Smart Structures and Materials 1996: Industrial and Commercial Applications of Smart Structures Technologies*, volume 2721. Virginia Polytechnic Inst. and State Univ., Blacksburg, VA, USA, pp. 26–37.

Furstoss, M., Thenail, D. and Galland, M. A. (Jun 5 1997) Surface impedance control for sound absorption: direct and hybrid passive/active strategies. *Journal of Sound and Vibration*, volume 203, no. 2, pp. 219–236.

Galland, M. A., Mazeaud, B. and Sellen, N. (2005) Hybrid passive/active absorbers for flow ducts. *Applied Acoustics*, volume 66, no. 6, pp. 691–708.

Griffin, J. R. (2006) The control of interior cabin noise due to a turbulent boundary layer noise excitation using smart foam elements.

Guigou, C. and Fuller, C. R. (Jul 1998) Adaptive feedforward and feedback methods for active/passive sound radiation control using smart foam. *Journal of the Acoustical Society of America*, volume 104, no. 1, p. 226.

Kundu, A. and Berry, A. (2010) Active control of transmission loss with smart foams. *submitted to Journal of the Acoustical Society of America*.

Kundu, A., Berry, A. and Leroy, P. (2009) Active control of broadband noise using smart foams. In *Proceedings of ACTIVE 2009*. Ottawa, Ontario, Canada.

Leroy, P. (2008) *Les mousses adaptatives pour l'amelioration de l'absorption acoustique : modelisation, mise en oeuvre, mecanismes de controle (Smart foams for the improvement of acoustic absorption: modeling, implementation, control mechanism)*. Ph.D. thesis, Université de Sherbrooke, Sherbrooke, Québec, Canada.

Leroy, P., Atalla, N. and Berry, A. (2009a) Three dimensional finite element modeling of smart foam. *Journal of the Acoustical Society of America*, volume 126, no. 6, pp. 2873–2885.

Leroy, P., Berry, A., Atalla, N. and Herzog, P. (2007) Numerical analysis of smart foam for acoustic absorption. In *19th International Congress on Acoustic*.

Leroy, P., Berry, A., Herzog, P. and Atalla, N. (2009b) Experimental study of a smart foam sound absorber. *submitted to Journal of the Acoustical Society of America*.

Mathur, G. P., Chin, C. L., Simpson, M. A. and Lee, J. T. (2001) *Structural Acoustic Prediction and Interior Noise Control Technology*. Technical Report NAS 1.26:211247; NASA/CR-2001-211247.

Moheimani, S. O. R. (2003) A survey of recent innovations in vibration damping and control using shunted piezoelectric transducers. *IEEE Trans-*

actions on Control Systems Technology, volume 11, no. 4, pp. 482–494. http://dx.doi.org/10.1109/TCST.2003.813371.

Peterson, C. D., Cazzolato, B. S., Zander, A. C. and Hansen, C. H. (2006) Active noise control at a moving location using virtual sensing. In *Proceedings of the 13th International Congress on sound and vibration.*

Peterson, C. D., Fraanje, R., Cazzolato, B. S., Zander, A. C. and Hansen, C. H. (2007) A kalman filter approach to virtual sensing for active noise control. *Mechanical Systems and Signal Processing*, volume 22, pp. 490–508.

Roure, A. and Albarrazin, A. (1999) The remote microphone technique for active noise control. In *Proceedings of Active '99.* pp. 1233–1244.

Tibbetts, G. C. (1977) Transducers having piezoelectric film arranged with alternating curvature. http://www.freepatentsonline.com/4056742.html.

Vipperman, J. and Clark, R. (1996) Implementation of an adaptive piezoelectric sensoriactuator. *AIAA Journal*, volume 34, no. 10, pp. 2102–2109.

Widrow, B. and Stearns, S. D. (1985) *Adaptive signal processing.* Prentice Hall.

Yuan, J. (Jun 1 2003) Causal impedance matching for broadband hybrid noise absorption. *Journal of the Acoustical Society of America*, volume 113, no. 6, pp. 3226–3232.